

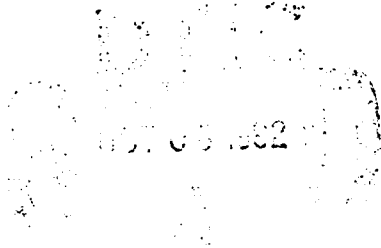
2

**AD-A256 370**



**Technical Report  
943**

**Sensors in Series: A Study of Sensors  
with Limited Traffic Capacity**



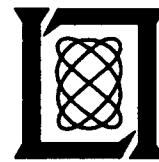
**S.M. Rocklin  
J.W. Tolleson**

**12 August 1992**

**Lincoln Laboratory**

**MASSACHUSETTS INSTITUTE OF TECHNOLOGY**

*LEXINGTON, MASSACHUSETTS*



Prepared for the Office of the Strategic Defense Initiative  
under Air Force Contract F19628-90-C-0002.

Approved for public release; distribution is unlimited.

92 10 5 087

207650

**92-26499**



59 px

This report is based on studies performed at Lincoln Laboratory, a center for research operated by Massachusetts Institute of Technology. The work was sponsored by the Office of the Strategic Defense Initiative under Air Force Contract F19628-90-C-0002.

This report may be reproduced to satisfy needs of U.S. Government agencies.

The ESC Public Affairs Office has reviewed this report, and it is releasable to the National Technical Information Service, where it will be available to the general public, including foreign nationals.

This technical report has been reviewed and is approved for publication.

FOR THE COMMANDER

*Hugh L. Southall*

Hugh L. Southall, Lt. Col., USAF  
Chief, ESC Lincoln Laboratory Project Office

*Non-Lincoln Recipients*

PLEASE DO NOT RETURN

Permission is given to destroy this document  
when it is no longer needed.



## EXECUTIVE SUMMARY

This report, which is an initial study of sensors in series, is directed at improving the performance of discrimination sensors with limited traffic capacity. The concept of a series network is discussed in detail in Section 3.1; limited traffic capacity is precisely defined in Section 2.2. Briefly, a sensor has limited traffic capacity if, because of energy or time constraints, the sensor is unable to measure all of the objects of interest and therefore must restrict its attention to a subcollection. If the subcollection to be scrutinized is determined beforehand based on measurements by another sensor, the two sensors are in series. If several sensors are arranged in this hierarchical pattern, they form a series network.

Another related arrangement of sensors is the parallel network, also described in Section 3.1. An arbitrary sensor network has an architecture that can always be defined in terms of smaller subnetworks, each of which is in a series or parallel arrangement. This report is a first step toward a quantitative description of how an arbitrary network performs. In designing any network, and in particular in this report for series networks, the following four issues are addressed.

1. **Global Performance:** How does the entire network perform, given the performance of each individual sensor?
2. **Sensitivity:** Given a fixed architecture, what is the effect of improving or degrading a single sensor?
3. **Performance Trade-offs:** How can the change in performance by the degradation of one parameter be offset by the enhancement of another?
4. **System Synthesis:** How does one construct a network to achieve a specified goal?

To fully address these issues for the two-sensor series network, an outline of the approach in Sections 2 through 4 is given as follows. The performance of a single sensor is modeled in a general setting independent of engineering constructs. Then the sensor is restricted to limit traffic capacity and to determine quantitatively the degradation in its performance. Next, the two basic types of network architectures, series and parallel, are defined and their primary attributes are delineated. Focusing then on the series arrangement, the basic measurement strategies are examined and their relative performances are evaluated. A theoretical basis for this approach is included in the appendices. Having chosen a measurement strategy, the performance trade-offs are studied between the key parameters defining the network for a two-sensor series arrangement. The quantitative results apply to a bulk filter and a precision sensor in series.

A general summary of the report includes the following points.

1. A new methodology is being developed that analyzes the performance of multiple sensor networks and calculates quantitatively the effects of perturbing key parameters in a network architecture.

2. The methodology is specialized to sensors with limited traffic capacity and series networks in this report but is currently being expanded to multiple sensors in arbitrary arrangements.
3. Traffic capacity is an important parameter that has significant effects on network performance. Lacking theoretical models, its effects have been only partly understood in the past. Traffic-limited sensors cannot be described by a single measure of quality such as a k-factor; rather, the entire leakage performance curve is required. This constraint also applies to sensors in series.

Some specific points of interest are detailed.

1. Low-quality sensors degrade slowly with traffic and are best used as bulk filters. High-quality sensors tend to degrade faster and are therefore more suited for traffic-limited precision sensors.
2. When combining two classes of sensors, either bulk or traffic-limited precision, or both, one of each in series performs best for small interceptor inventories.
3. When traffic capacity is limited, bulk filters are required. Hard lower limits on bulk filter quality ( $k_1$ ) are necessary to achieve low leakage; also, a hard lower limit on interceptor inventory is required.
4. In a series arrangement, the precision sensor has required minimal values for both sensor quality ( $k_2$ ) and traffic capacity. Both of these parameters have hard lower bounds.

## **ACKNOWLEDGMENTS**

The authors wish to thank Steve Weiner for his continued support throughout the evolution of this problem. We also wish to thank Donna McTague for her assistance on a very difficult manuscript.

## TABLE OF CONTENTS

Executive Summary	iii
Acknowledgments	v
List of Illustrations	ix
1. INTRODUCTION AND MOTIVATION	1
2. SINGLE SENSOR WITH LIMITED TRAFFIC CAPACITY	3
2.1 Single Sensor Performance	3
2.2 Single Traffic-Limited Sensor	6
3. SENSORS IN SERIES	11
3.1 Series and Parallel Arrangements	11
3.2 Traffic Thresholds	11
4. NUMERICAL RESULTS	19
4.1 Performance Analysis	19
4.2 Trade-off Analysis	21
5. SUMMARY	29
APPENDIX A. A COMPARISON OF TRAFFIC-LIMITED AND CONTINUOUSLY DEGRADED SENSORS	31
APPENDIX B. DERIVATION OF THE BASIC DENSITY FUNCTION FOR A CHAIN OF SENSORS IN SERIES	39
APPENDIX C. LOG-LIKELIHOOD RATIO AS A DECISION FUNCTION	43
APPENDIX D. THE SYNCHRONIZED FIRING THRESHOLD	47
REFERENCES	51

## LIST OF ILLUSTRATIONS

Figure No.		Page
1	Human retina: a sensor series in nature.	2
2	Single sensor function.	4
3	Single sensor quality.	5
4	Single sensor with limited traffic capacity.	7
5	Performance curves for a traffic-limited sensor.	8
6	Two basic networks.	12
7	Two sensors: no traffic constraint.	13
8	Dual threshold model.	14
9	Single threshold model.	15
10	Comparison of dual and single threshold models.	17
11	Performance of two sensors in series.	20
12	Sensor substitution performance.	21
13	Sensor quality trade-off: leakage fixed.	22
14	Sensor quality trade-off: traffic fixed.	23
15	Precision sensor trade-off.	24
16	Traffic/inventory trade-off.	26
17	Bulk filter/precision sensor trade-off.	27
A-1	Continuous degradation traffic model.	31
A-2	Performance curves for fixed limit and continuous models.	33
A-3	Comparison of fixed limit and continuous models.	34
A-4	Generalized-continuous model.	35
A-5	Performance of generalized-continuous model.	37
B-1	Region of feature space passed on to sensor $S_3$ .	40
C-1	Optimal and nonoptimal decision regions.	44
D-1	Discontinuous density functions induced by a traffic threshold.	48
D-2	Synchronized firing thresholds.	50

## 1. INTRODUCTION AND MOTIVATION

The problem of a sensor suffering a degradation of performance because of limited traffic capacity is as old as mankind itself — in fact, older. Nature has found numerous ways of dealing with this problem; many sensors perform their tasks so efficiently and smoothly that their details often go unnoticed. Yet all of them fall into two general categories: (1) two or more sensors measuring physically different modalities and operating in parallel or (2) two or more sensors in a series hierarchy with one member restricting the flow of information to the others. The human eye is an example of a series network of sensors.

The layer of receptor cells making up the human retina consists of two types: rods and cones. Almost all of the cones (90 percent) populate the central part of the retinal focal plane, which is called the fovea; see Figure 1. The cones form a high-quality discriminator, a precision sensor, that sees color, shape, and texture. To classify an object — that is, to know exactly what it is — the image must be brought to the very center of the visual field of the fovea. At this point the eye quickly scans the object using thousands of saccadic swings in azimuth and elevation on the order of seconds of arc. Once classified, the image can be shifted off the fovea, where the remaining 10 percent of the cones keep the image under surveillance. This is a time-consuming job, and while it goes on, the remaining field of view is watched by the system of rods. Rods cannot discriminate very well, but they are excellent detectors of motion and changes in light intensity; they form an efficient bulk filter. Without their parallel surveillance of the periphery of the visual field, our eyes would constantly be swinging around like a spotlight in the sky, darting from *place to place without a directing mechanism*. The system of rods not only tells us what to look at but also what not to bother looking at. It manages the flow of traffic to the fovea. The rod and cone systems of the retina are the preeminent example of a bulk filter and a traffic-limited precision sensor in series.

In problems related to discrimination architecture, the main concern in this report, the reasons for constructing sensor networks can be quantified in terms of the particular sources of error of the sensors. The first source is measurement error: the sensor may inherently operate with a high level of noise/signal. If the same object is measured repeatedly by the same sensor, a large amount of variation is seen in the measurement values. The second source is physics error: the sensor can only measure a single physical attribute. If two distinct objects are measured by the same sensor, their difference will be smaller than if measured by several sensors using different modes of measurement. (This is not unlike Plato's allegory of the blind men and the elephant.) The third source is traffic error: a sensor's performance can be degraded by the sheer number of objects that it must measure. If the sensor has only limited time or energy to measure all objects, then the amount that it can devote to each object is reduced.

Physics error and measurement error are generally remedied by having two or more sensors measure every object. Such an arrangement is called a parallel network. Traffic error, on the other hand, is remedied by having a set of early sensors act as a bulk filter to restrict the number of objects passed on to be measured by a set of precision sensors. In effect, the bulk filter directs the attention of the precision sensor to only a small subset of the total traffic. This arrangement is called a series network, and this particular class of network is the focus of this report.

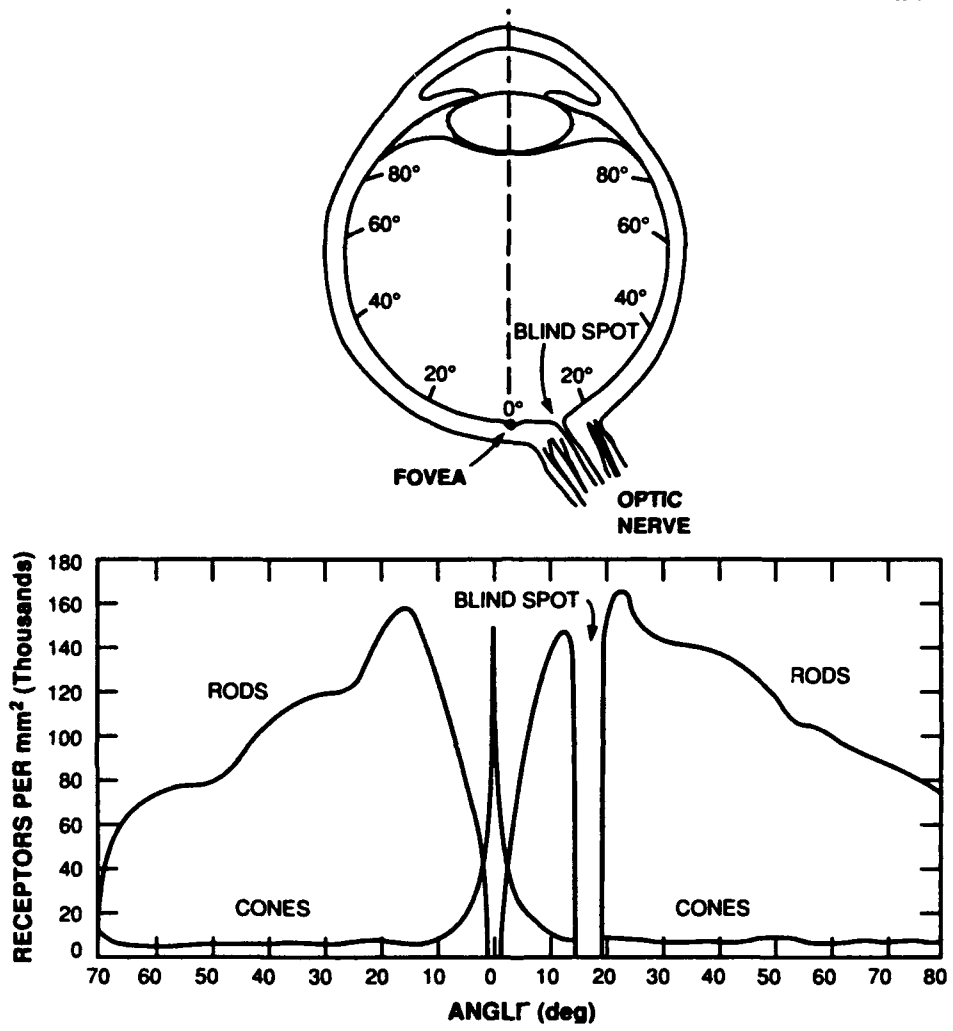


Figure 1. Human retina: a sensor series in nature.

## 2. SINGLE SENSOR WITH LIMITED TRAFFIC CAPACITY

In this section the serious degradation of a sensor's performance by limited traffic capacity is detailed. By concentrating on a single sensor we not only motivate the need for construction of sensor networks but also establish a few important relationships between traffic capacity and system leakage that will be used throughout the remainder of the report. As a point of reference we begin by looking at a sensor without traffic limits.

### 2.1 SINGLE SENSOR PERFORMANCE

In this section, the performance characteristics of a typical sensor will be discussed, rather than the details of how it is constructed or how it carries out its measurement processes. Accordingly, a sensor will be defined by the probability densities of its measurements along some discriminant axis  $x$ , as shown in Figure 2. Two response densities,  $p_R(x)$ , and  $p_D(x)$ , that correspond to whether the object being measured is an RV or a decoy are shown. Alternatively, the assumption could be made that if a large population of objects was measured, they would distribute themselves according to some probability law, based on measurement uncertainty, as shown in the figure. We will often take this latter point of view.

Given a threat consisting of a certain number of RVs and decoys and an interceptor inventory of size  $I$ , what is the best rule for choosing the objects to fire at based only on the discriminant  $x$ ? The optimal rule yielding the minimum expected leakage is obtained by choosing a threshold  $\eta$  and firing at only those objects whose discriminant lies above  $\eta$ . This rule is derived under more general circumstances in Appendix C. The most important characteristic of the optimal rule is that the threshold depends only on the degree of belief that an object is an RV or a decoy and that that degree of belief is captured by a single quantity known as the likelihood ratio

$$\Lambda(x) = p_R(x) / p_D(x)$$

or, equivalently, the log-likelihood ratio (LLR)

$$L(x) = \log \left[ p_R(x) / p_D(x) \right] .$$

One of the principal advantages of the log-likelihood ratio as a decision criterion is that it extends in a straightforward way to multiple sensors [1] (see Section 2.2).

The quality of the sensor is measured by the degree of separation of the response densities on the discriminant axis or, equivalently, by the leakage/false alarm rates. The leakage  $P_L$  is the fraction of RVs classified as decoys and hence leak through the system because they are not fired at. The probability of false alarm  $P_F$  is the fraction of decoys classified as RVs and hence have valuable interceptors fired at them. Referring to Figure 2 and the threshold  $\eta$ ,  $P_L$  and  $P_F$  are given by

$$P_L(\eta) = \int_{-\infty}^{\eta} p_R(x) dx \quad \text{and}$$
$$P_F(\eta) = \int_{\eta}^{\infty} p_D(x) dx .$$

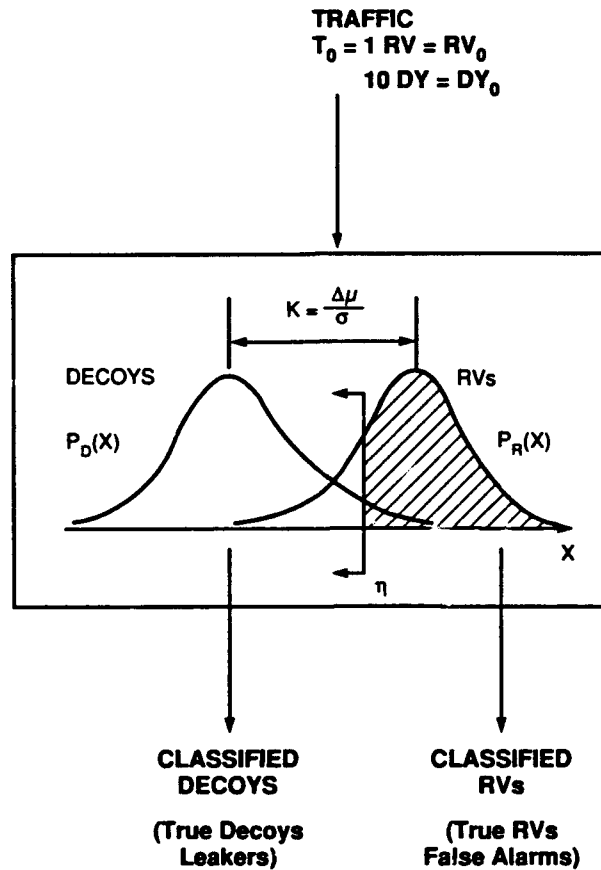


Figure 2. Single sensor function.

Another equivalent way of measuring sensor quality is by the leakage/inventory performance. For a given threshold  $\eta$ , the number of interceptors fired  $I_0$  is equal to the number of objects classified as RVs, that is, the number of objects whose discriminant  $x$  is greater than the threshold  $\eta$ :

$$I_0 = [1 - P_L(\eta)] RV_0 + P_F(\eta) DY_0 \quad ,$$

where  $RV_0$  and  $DY_0$  are the number of RVs and decoys in the initial threat. For any given number of interceptors fired, sensor A is better than sensor B if  $P_{LA} < P_{LB}$ .

For sensors whose response densities are given by Gaussian distributions (with equal variances  $\sigma$ ), the density functions yield a numerical measure of quality known as the sensor's k-factor. Such sensors are known as classical Gaussian sensors. The k-factor is given by

$$k = (\mu_R - \mu_D) / \sigma \quad ,$$

where  $\mu_R$  and  $\mu_D$  are the means of the RV and decoy densities, respectively.

This numerical measure translates directly into a leakage/inventory ( $P_L$  vs  $I$ ) performance measure, which is seen in Figure 3(a). As an example an initial normalized threat  $T_0 = (RV_0, 10 RV_0)$  is assumed, which consists of ten decoys per RV. As the number of (hypothetically perfect) interceptors in the inventory increases from zero to  $T_0$ , the system leakage drops from  $P_L = 1.0$  to  $P_L = 0.0$  for all of the curves. For any intermediate point on the  $I$  axis, the higher the  $k$ -factor, the lower the value of  $P_L$ . For  $k = 0$  the performance curve is a straight line, referred to as the "chance line." This line corresponds to the case where no discrimination is possible and, consequently, objects are chosen at random to be fired at.

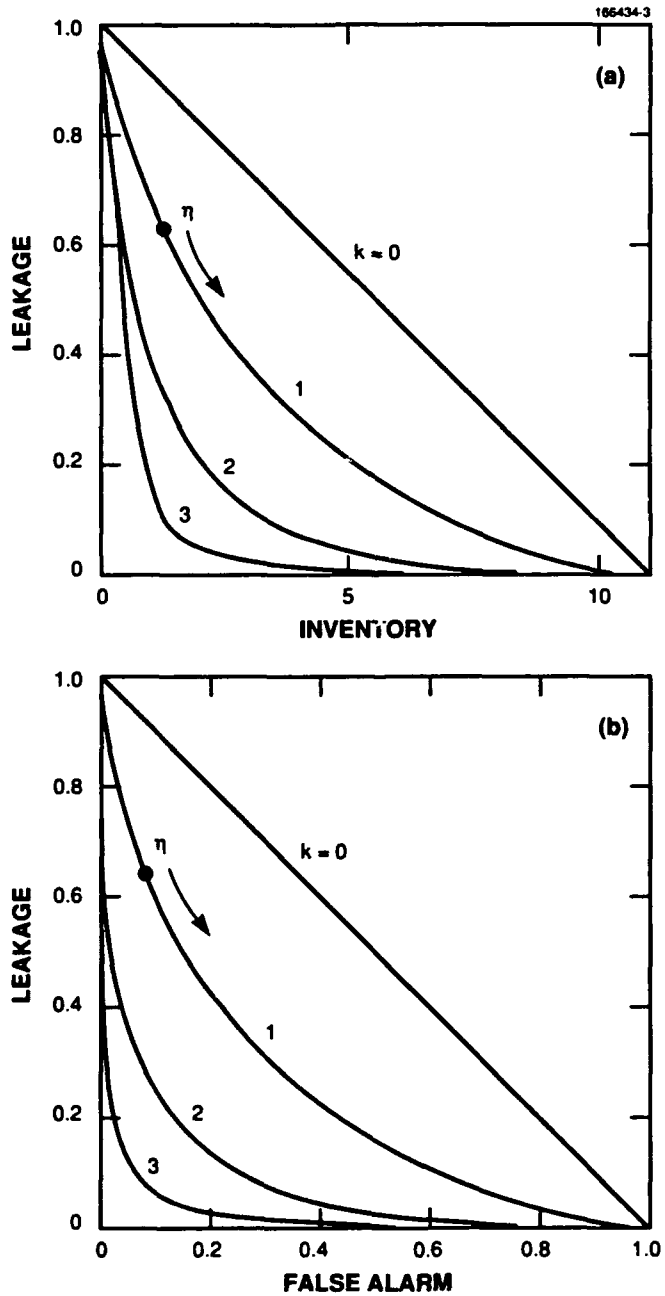


Figure 3. Single sensor quality.

The sensor performance curve, whether  $P_L$  vs  $I$  or  $P_L$  vs  $P_F$ , as shown in Figure 3(b), is a more fundamental measure of sensor quality than the k-factor because it applies to all sensors, Gaussian or not. As traffic-limited sensors are considered, the  $P_L$  vs  $I$  curves used to compare the quality of various sensors and sensor networks are more complex. The advantage of classical Gaussian sensors, whenever they are used, is that their quality can be summarized by a single number: the k-factor.

## 2.2 SINGLE TRAFFIC-LIMITED SENSOR

Traffic, as used in this report, is the total number of objects that a sensor must measure in order to perform discrimination. Traffic in the context of degrading the performance of the sensor is of particular interest. If the size of the threat  $T_0$  is not large enough to affect the sensor's performance, then the sensor has, in effect, an infinite traffic capacity. If the amount of traffic can degrade performance, then the sensor has limited traffic capacity.

The presence of high traffic can cause a sensor's performance to degrade in one of two ways. First, the sensor measures all of the objects but must ration its energy (number of pulses or signal duration) in doing so. Its measurement accuracy will then go down uniformly across all objects in a manner consistent with the results of statistical sampling theory. This form of performance degradation is referred to as continuous degradation; it is presented in Appendix A but will not be discussed in detail in this report.

In contradistinction to uniform degradation is a strictly limited sensor — one that does not or cannot measure more than a limited number of objects  $T_1$ . The traffic capacity of the sensor is denoted by  $T_1$ . If the threat size  $T_0$  exceeds  $T_1$ , then  $T_1$  objects can be measured by the sensor; from the remaining  $T_0 - T_1$  objects, interceptor allocation must be made by random selection alone, which is denoted as random discrimination. Figure 4 shows a single  $P_L$  vs  $I$  performance curve and a schematic diagram demonstrating how the curve is obtained. In Figure 5 a family of such curves, parameterized by traffic capacity, is displayed.

First, a subpopulation of  $T_1$  objects is flagged at random to be measured by the sensor  $S_1$ . Notice that the prior probabilities ( $P_R, P_D$ ), the fraction that are RVs and the fraction that are decoys, are the same within the two subpopulations  $T_1$  and  $T_0 - T_1$ , as in the original threat. This similarity exists because of the random selection of  $T_1$ . The RV and decoy density functions,  $p_R(x)$  and  $p_D(x)$ , are also the same for populations  $T_1, T_0 - T_1$ , and  $T_0$ . To generate the performance curve of Figure 4, we begin in the upper left corner with the inventory at zero and the leakage at one. As the inventory increases from zero, the most RV-like of the objects in population  $T_1$  are designated by a threshold  $\eta$  that moves in from the right. All objects with measurements larger than  $\eta$  are classified as RVs, with  $\eta$  chosen such that the total number of such objects, true RVs and false alarms, matches the total inventory. When the inventory increases to  $T_a$  and  $\eta$  reaches the critical value  $\tau_a$ , discrimination now takes place by choosing, at random, objects from the  $T_0 - T_1$  subpopulation of unmeasured objects. The critical value  $\tau_a$  is located so that the marginal rate of RVs chosen correctly from population  $T_1$  per unit increase in inventory is equal to the marginal rate achieved by randomly choosing objects from  $T_0 - T_1$ . This value occurs when the marginal rate from  $T_1$  equals the marginal rate from  $(T_0 - T_1)$ , that is, when

$$RV_1 P_R(\tau_a) / DY_1 P_D(\tau_a) = P_R / P_D$$

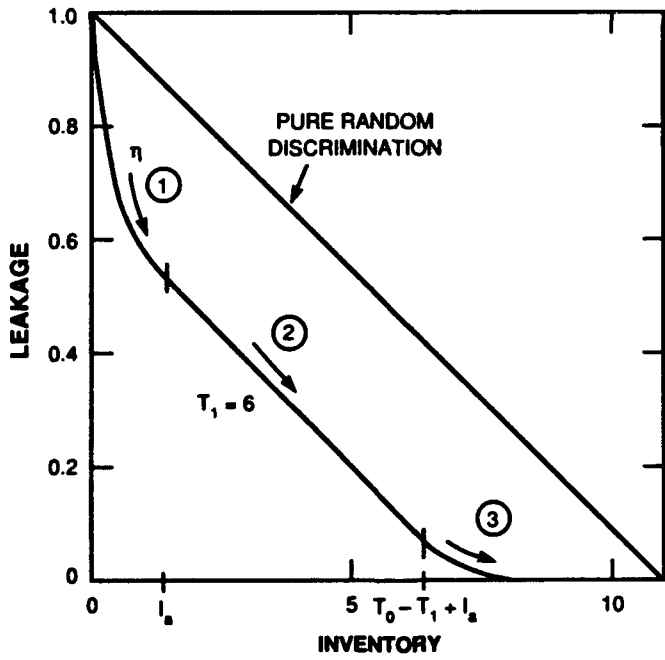
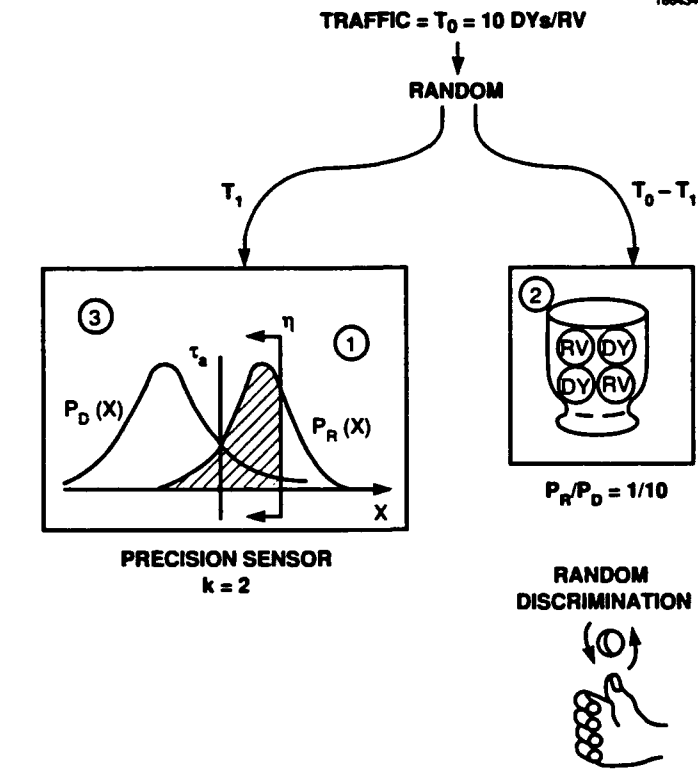


Figure 4. Single sensor with limited traffic capacity.

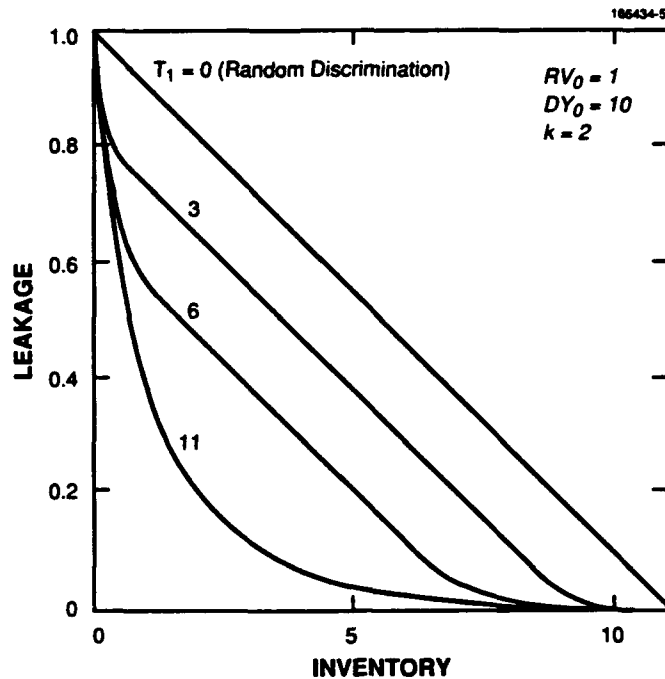


Figure 5. Performance curves for traffic-limited sensor.

or

$$P_R(\tau_a)/P_D(\tau_a) = 1 .$$

Thus, the critical threshold is located where the RV and decoy density curves cross each other.  $RV_1$  and  $DY_1$  are the number of RVs and decoys in population  $T_1$ . However, because of the random partitioning of  $T_0$  into the two subpopulations,  $RV_1/DY_1 = RV_0/DY_0 = P_R/P_D$ .

To summarize thus far, sensor  $S_1$  has classified objects whose discriminant lies above  $\tau_a$  from the RV-rich portion of  $T_1$ . What is left from  $T_1$  is now an RV-poor, decoy-rich subpopulation. In fact,  $T_1$  has been so depleted of RVs that the interceptors can be used more efficiently if we now abandon, temporarily, population  $T_1$  and start firing at population  $T_0 - T_1$  at random. Thus, for higher values of inventory  $I > T_a$ , excess interceptors are now directed at objects in  $T_0 - T_1$ .

The rate of decrease in  $P_L$  now follows parallel to the chance line, which is consistent with RVs being selected at random. Note that the initial portion of the performance curve has the same slope as the chance line when the switch to the random subpopulation takes place which indicates their equal marginal rates of decrease in  $P_L$ . As inventory increases, objects are chosen from the subpopulation  $T_0 - T_1$  until exhaustion. At that point, when the inventory increases above  $T_0 - T_1 + T_a$ , discrimination switches

back to the remainder of population  $T_1$ . Objects whose discriminant lies to the left of  $\tau_a$  are chosen by moving the threshold  $\eta$  downward from  $\tau_a$ , again picking the most RV-like. On the performance curve the marginal rate of decrease of  $P_L$  is now less than the chance line, reflecting that the remaining RV population has been thinned out relative to the whole.

Figure 5 contains an array of performance curves as  $T_1$  takes the values 0, 3, 6, and 11 (11 is the size of our normalized threat).  $T_1 = 0$  coincides with the chance line corresponding to random selection over the entire threat  $T_0$ .  $T_1 = 11$  implies no traffic limitations are in effect for this threat, which corresponds to the standard performance curve for a sensor with a k-factor of  $k = 2.0$ . Notice the dramatic degradation of performance in the form of an increase in  $P_L$  as traffic capacity drops. What is more important here is that this degradation shows up at relatively low values for inventory  $I \approx RV_0$ ; limited traffic capacity hurts the defense most for small inventories. An antidote to this problematic situation is to precede a traffic-limited sensor with a bulk filter (i.e., to form an elementary series network).

### 3. SENSORS IN SERIES

#### 3.1 SERIES AND PARALLEL ARRANGEMENTS

The equal spacing of the performance curves for the single traffic-limited sensor shows in a striking fashion that the price paid in increasing leakage is proportional to the traffic capacity. This spacing motivates us to ask how much can be gained by preceding a precision sensor  $S_2$  (e.g.,  $k \geq 2.0$ ), whose traffic capacity is limited, by a modest bulk filter  $S_1$  (e.g.,  $k = 1.0$ )? Figure 6(a) illustrates this series arrangement of two sensors. Each sensor takes a measurement of an object and generally makes a ternary decision of the form RV/DY/UN, where UN stands for "uncertain." A UN classification means that the full measurement is retained by the sensor to be used later in a decision process. If  $S_1$  precedes  $S_2$  (or, equivalently,  $S_2$  follows  $S_1$ ) in a series arrangement, then two characteristics emerge: (1) any classification into either RV or DY by sensor  $S_1$  is final and cannot be overridden by  $S_2$  and (2) only the measurements of objects classified as uncertain by sensor  $S_1$  are handed over to sensor  $S_2$  for further measurement. This process defines a natural order of sensors in a series of any length.

No such order exists in a parallel arrangement, as shown in Figure 6(b), where full measurement information is available to every sensor on every object. Only after all measurements on all objects are made is this information collected in a data-fusion center where a classification process is carried out. Further discussion of parallel networks can be found in Holmes and Rocklin's research [1,2].

In the series chain illustrated in Figure 6(a), each object labeled either  $RV_i$  or  $DY_i$  has been culled from a population previously classified as uncertain by sensor  $S_{i-1}$  and passed on to sensor  $S_i$ . The decision to classify an object as either RV or DY by sensor  $S_i$  must therefore be based on a feature vector  $(x_1, x_2, \dots, x_i)$  consisting of measurements by only the earlier sensors in the chain. The total number of objects classified as uncertain by sensor  $S_{i-1}$  is generally constrained to be equal to the traffic capacity of sensor  $S_i$  and is therefore denoted  $T_i$ .

#### 3.2 TRAFFIC THRESHOLDS

The convention discussed in Section 3.1 is denoted by the double threshold model because each sensor separates its individual feature space by a pair of traffic thresholds into the three decisions: RV/DY/UN. There are two special cases: the single threshold model that divides feature space into DY/UN and the full measurements case in which all objects are measured and classified UN until the final sensor. These three models are contrasted schematically in Figures 7, 8, and 9.

The full measurements or "no traffic threshold" case corresponds to all sensors in parallel with no traffic limitations. For  $m$  such sensors, the full measurement model decides on an RV or a decoy based on the full feature vector  $(x_1, x_2, \dots, x_m)$ . The actual decision is based on the likelihood ratio (LLR) for multiple sensors:

$$\Lambda(x_1, \dots, x_m) = p_R(x_1, \dots, x_m) / p_D(x_1, \dots, x_m) \underset{DY}{\overset{RV}{\geq}} \eta \quad .$$

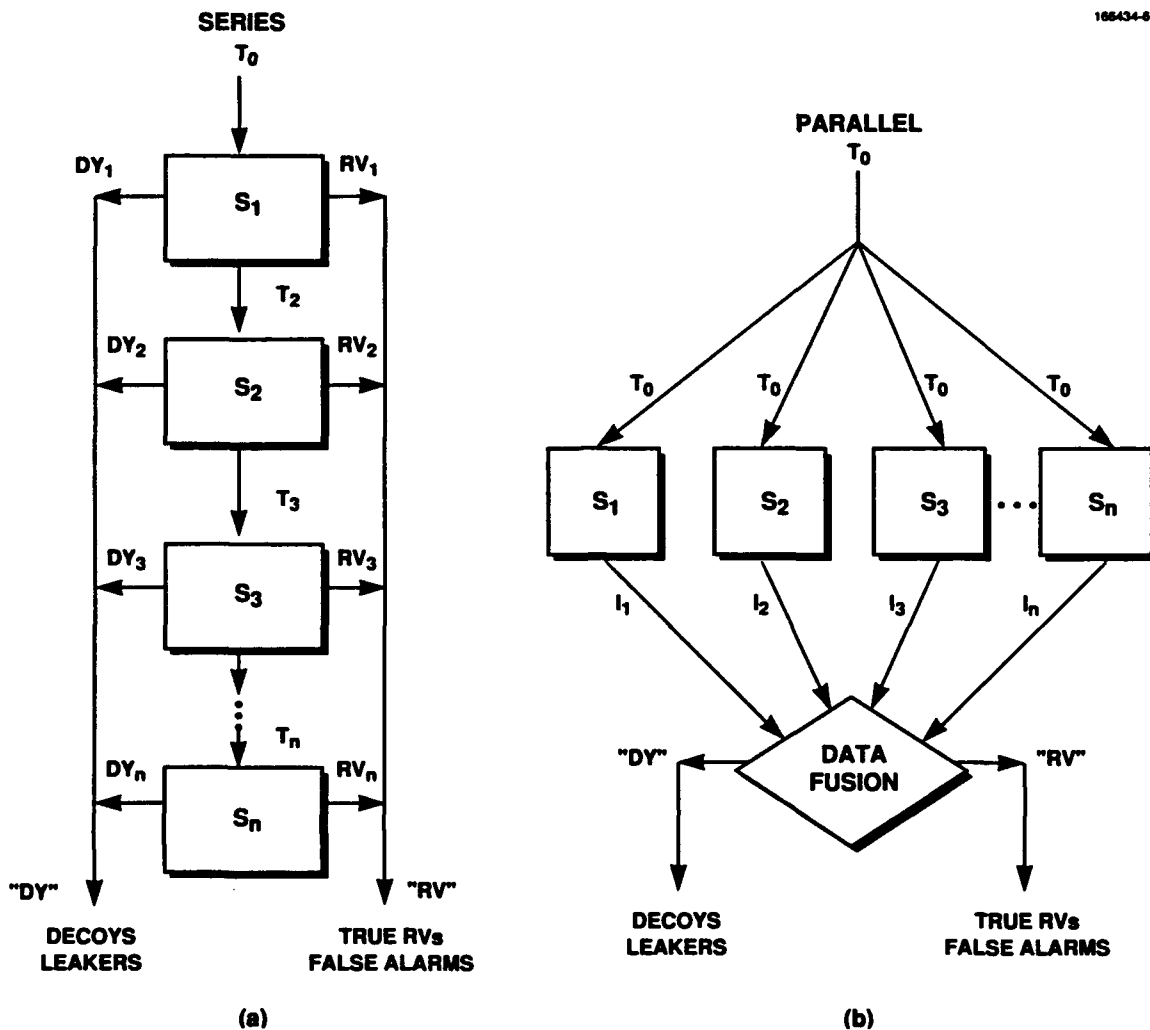


Figure 6. Two basic networks.

Thus, if the LLR exceeds a certain threshold  $\eta$ , classify the object as an RV; otherwise, classify it as a decoy. See Appendix C for a derivation. The factor  $\eta$  is a preset threshold that will depend on a given interceptor inventory level. For two Gaussian sensors this threshold corresponds to the familiar hyperplane threshold that lies perpendicular to the line connecting the peaks of the RV and decoy density functions, which is illustrated in Figure 7. This material is well studied, appears in a variety of reports, and will not be discussed further except to add that the combined or joint  $k$ -factor for  $m$  Gaussian sensors in parallel is the root-sum-square of the individual  $k$ -factors:

$$k_{\text{com}} = (k_1^2 + k_2^2 + \dots + k_m^2)^{1/2} \quad (1)$$

The dual threshold model is shown in detail in Figure 8. Let  $x_1$  represent the discriminant for sensor  $S_1$  and  $x_2$  represent the discriminant for sensor  $S_2$ . The classification scheme for two sensors and how the results extend to several sensors in series will be discussed. In the figure the equiprobable contour curves (circles) are shown for a pair of independent classical Gaussian sensors. A generalization to non-Gaussian sensors is under current investigation.

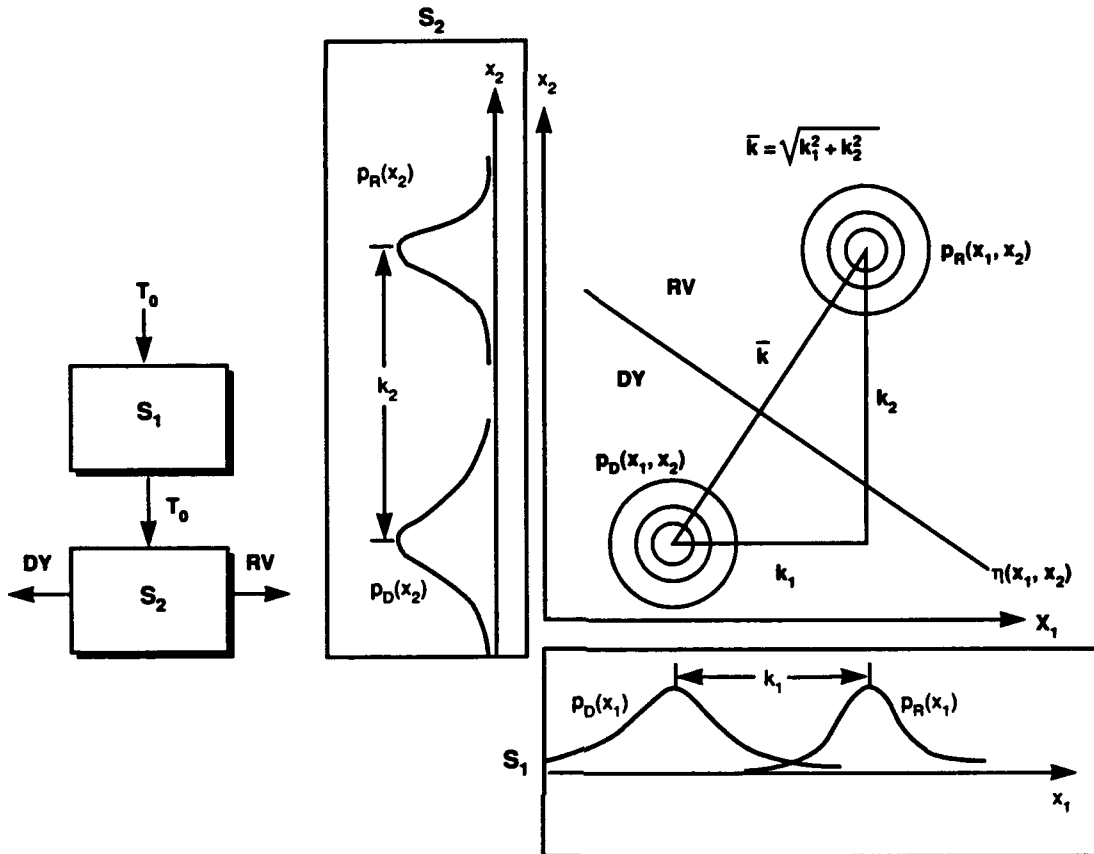


Figure 7. Two sensors: no traffic constraint.

Consider sensor  $S_1$  alone. Its RV and decoy density functions are shown along the  $x_1$  axis. Because  $S_2$  is traffic limited, a pair of traffic thresholds ( $\tau_{a1}$ ,  $\tau_{h1}$ ) is chosen on the  $x_1$  axis in such a way that the expected total population of objects, RVs and decoys, whose discriminant lies between  $\tau_{a1}$  and  $\tau_{h1}$  is precisely equal to  $T_2$ , the traffic capacity of sensor  $S_2$ .  $S_1$  classifies these objects as uncertain  $UN_1$ . Objects whose discriminant lies below  $\tau_{a1}$  or above  $\tau_{h1}$  are classified by  $S_1$  as decoys or RVs, respectively. They are denoted by  $DY_1$  and  $RV_1$ . Only the objects classified  $UN_1$  will be measured again by sensor  $S_2$ , and for these objects a final classification into RVs and decoys,  $RV_2$  and  $DY_2$ , will be made based on the joint discriminant  $(x_1, x_2)$ . The final threshold is based on the joint LLR and therefore is a truncated version of the full measurements threshold of Figure 7. After the final classification, the entire feature space is partitioned into RVs ( $RV_1 + RV_2$ ) and decoys ( $DY_1 + DY_2$ ).

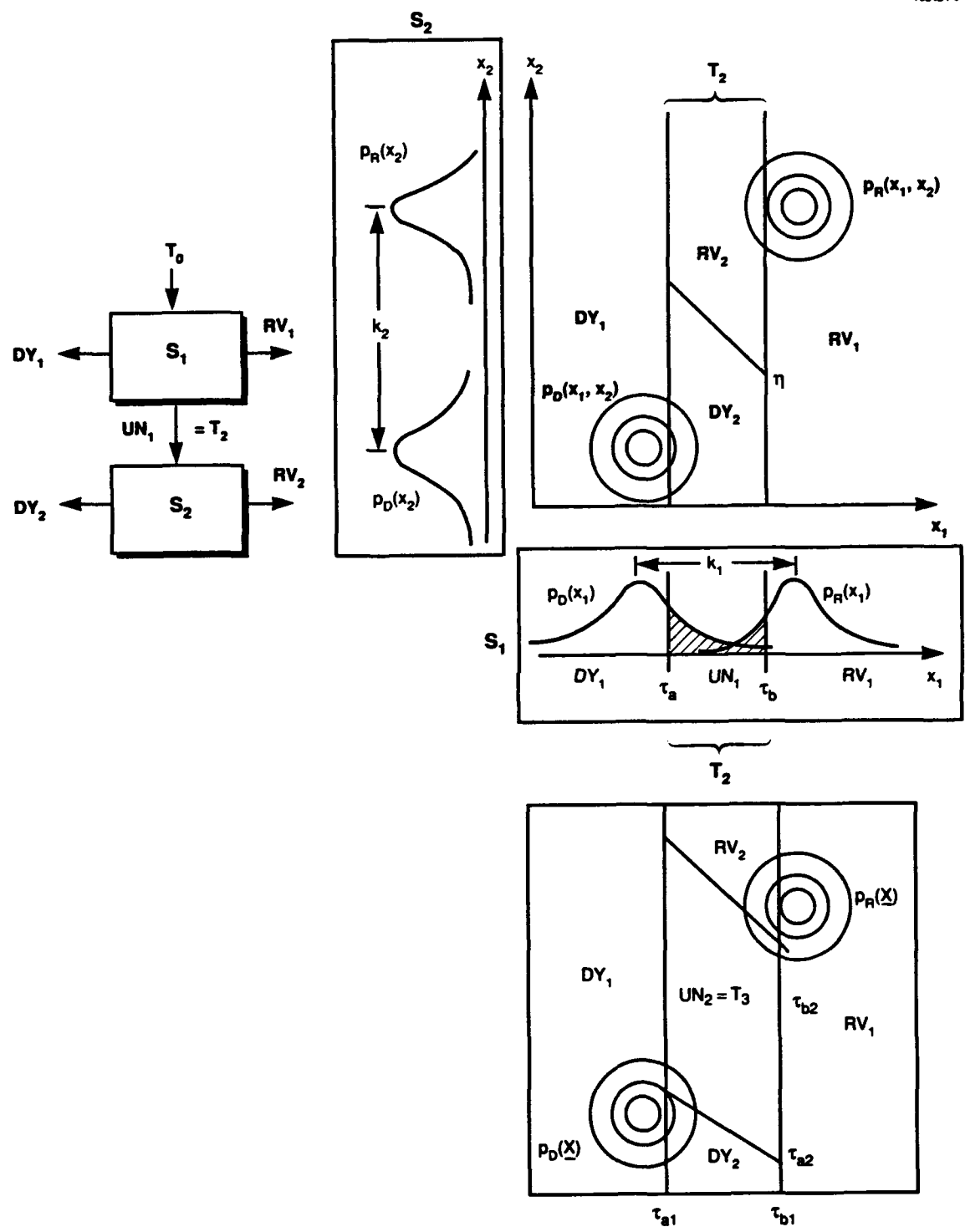


Figure 8. Dual threshold model.

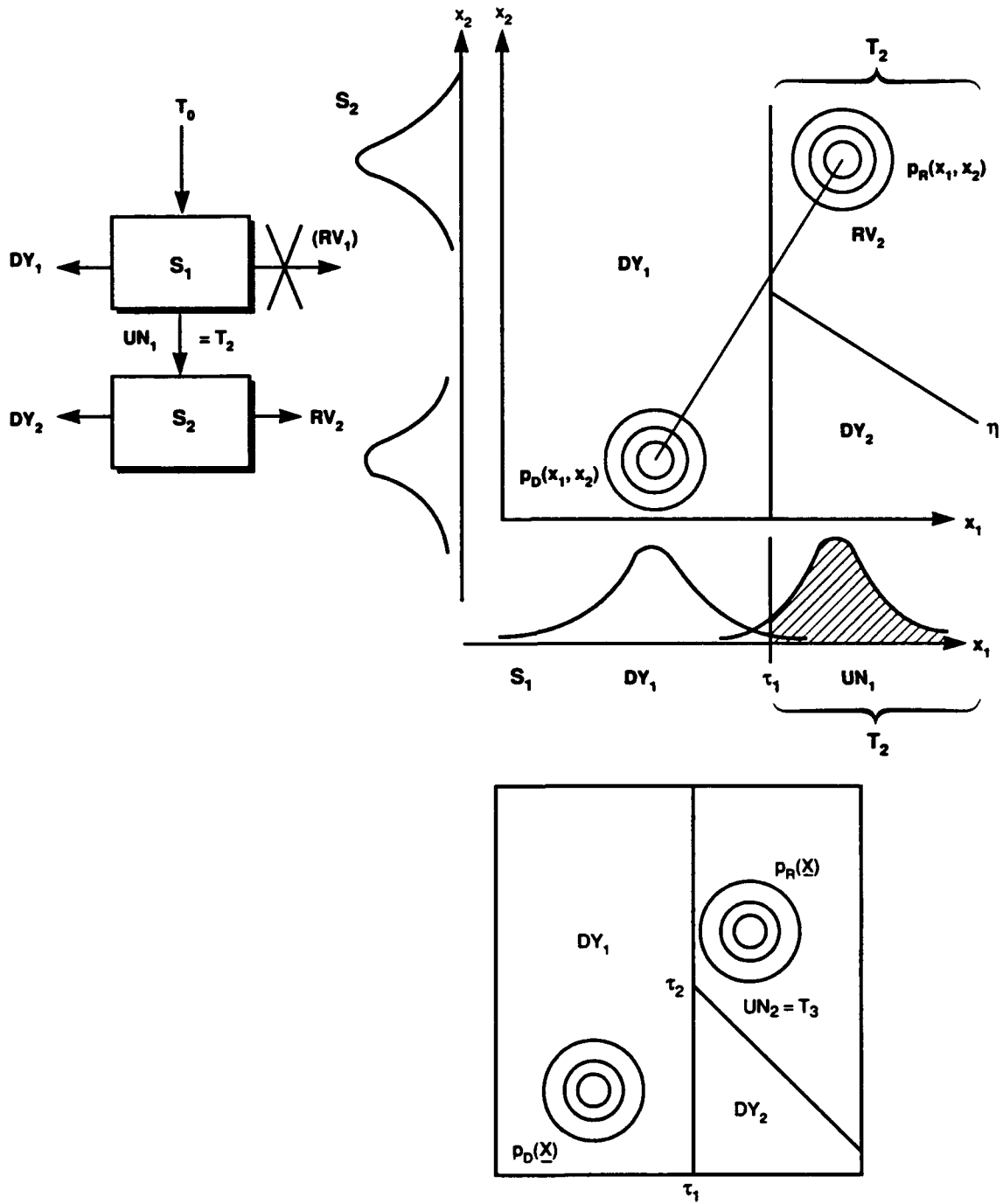


Figure 9. Single threshold model.

parallelogram-shaped region in the lower figure of Figure 8. As this process continues sequentially for all of the sensors in the chain, successively higher and higher dimensional paralleloprisms are formed, each being fed by objects within a similar prism of one lower dimension. The final classification will take place on some  $m$ -dimensional prism. To compute leakages and false alarms, the joint distribution of all objects classified as uncertain by sensors  $(S_1, S_2, \dots, S_m)$  for any  $m$  must be determined. The joint density is developed in Appendix B.

There is one major difficulty with the dual threshold model — the traffic thresholds  $\tau_a$  and  $\tau_h$  are not uniquely determined. That is, there are many pairs of thresholds  $(\tau_a, \tau_h)$  for sensor  $S_1$  (or any sensor  $S_i$  in the chain for that matter) such that the number of objects lying between the two thresholds equal  $T_2$ . In other words, the traffic capacity  $T_2$  determines the width of the traffic window but not its location. The optimal window location (as measured by its right-hand endpoint  $\tau_h$ , for instance) depends on many parameters in the system, but in particular it is inventory dependent. As such, it must be numerically optimized for each point on the  $P_L$  vs  $I$  performance curve. The dependence of the optimal window on interceptor inventory falls into the general research area of optimal measurement strategies, which is under current investigation.

A special case of the dual threshold model is the single threshold model, as shown in Figure 9. The single threshold  $\tau$  corresponds to  $\tau_a$ , the left-hand endpoint of the dual threshold measurement window with the right-hand endpoint at infinity, and serves to classify objects as either decoy or uncertain with the uncertain objects going on to sensor  $S_2$  for further measurement. The traffic constraint ( $UN_1 = T_2$ ) must be satisfied; that is, the total number of objects whose discriminant lies to the right of  $\tau$  must be equal to the traffic capacity of sensor  $S_2$ . Because the right-hand endpoint of the measurement window lies at infinity and the left endpoint is fixed by the traffic constraint, no inventory-dependent optimization is performed in this case.

The objects classified as uncertain  $UN_1$  are passed to sensor  $S_2$ , measured again, and are finally classified as RVs or decoys based on the joint LLR. So, for two sensors in series, the entire feature space is partitioned into RVs ( $RV_2$ ) and decoys ( $DY_1 + DY_2$ ). If instead these two sensors precede a third sensor in the chain, then the objects measured by sensor  $S_2$  are classified as either  $DY_2$  or  $UN_2$  and must satisfy the traffic limit of sensor  $S_3$ ,  $UN_2 = T_3$ . This situation is shown in the lower figure. The density function for objects classified as uncertain, derived in Appendix B, remains valid for the single threshold model. The limits of integration must be modified to take into account that the appropriate regions are now semi-infinite wedges rather than paralleloprisms.

The fact that the traffic window is uniquely determined in the single threshold model is very important. For multiple sensors in series, this determination yields a tremendous amount of computational savings. In a series chain of  $n$  sensors, the dual threshold model requires  $n - 1$  coupled numerical optimizations to find the traffic windows taking place concurrently with an LLR test to determine the appropriate firing threshold. For the single threshold model, the traffic thresholds can be solved for uniquely at the beginning before the firing thresholds are determined.

Figure 10 shows the amount of lost performance in switching from a dual threshold to a single threshold model for two sensors in series. A threat of ten decoys per RV is considered with sensor k-factors of  $k_1 = 1$  and  $k_2 = 2$ . Each curve represents the performance of a dual threshold measurement rule for some fixed traffic capacity of sensor  $S_2$ . Rather than optimize the location of the traffic window, it is used as a variable along the abscissa.  $RV_1/I = 0$  means no objects are classified as RVs by the first sensor; the traffic window is as far to the right as possible along the  $x_1$  discriminant axis. This point corresponds to the single threshold rule.  $RV_1/I = 1$  means that the traffic window is as far to the left on the  $x_1$  axis as possible; the number of objects classified as RVs by  $S_1$  just matches the inventory level. Because all of these objects must be fired at, using up the entire inventory, the traffic passing on to sensor  $S_2$  has no effect on the network performance — the performance is that of a single sensor with a k-factor of  $k = k_1 = 1$ .

These two endpoints represent the extremes in the location of the traffic window. The optimal location, as the curves indicate, is an internal minimum, running from  $RV_1/I \approx 0.70$  for  $T_2 = 1$  to very close to  $RV_1/I = 0.0$  for higher values of  $T_2$ . The difference in performance is about 4 percent for the worst case  $T_2 = 1$  and becomes negligible for values of traffic capacity  $T_2 \geq 3$ . Because of the great savings in computation and the small cost in performance, the single threshold model will be used in the rest of this report.

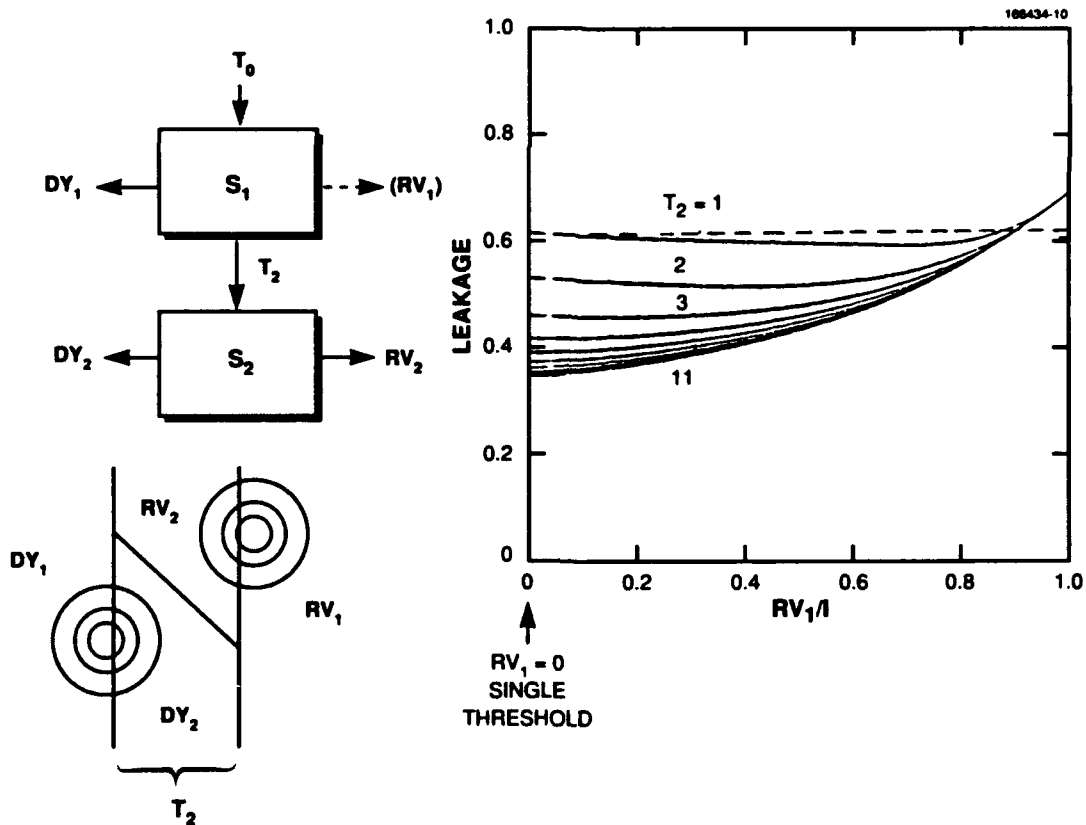


Figure 10. Comparison of dual and single threshold models.

## 4. NUMERICAL RESULTS

In this section the ramifications of placing a modest bulk filter in series with a precision sensor of limited traffic capacity are examined. The key parameters and attributes that are the focus of attention are listed in Table 1. The results presented here pertain to a pair of classical Gaussian sensors. Extension to more general sensors and to series chains containing an arbitrary number of sensors is under investigation.

**TABLE 1**

**Key Parameters**

• Sensor 1:	Quality $k_1$	
• Sensor 2:	Quality $k_2$	
	Traffic Capacity $T_2$	
• Interceptors:	Inventory $I$	
• Performance:	Leakage vs $I$	
• Trade-offs:	Quality:	$k_1$ vs $k_2$ } Fixed $P_L$
	Sensor 2:	$k_2$ vs $T_2$ } Fixed $T_2$
	Quantity:	$I$ vs $T_2$
	Sensors:	$k_1$ vs $T_2$

In addition to the usual parameters — sensor quality as measured by the individual k-factors and size of interceptor inventory — the key parameter in these results is the traffic capacity of the precision sensor  $T_2$ . We assume that the bulk filter has infinite traffic capacity as far as the threat is considered. Our interests are: (1) What is gained by putting a bulk filter in series with a precision sensor as compared to a bulk filter or a precision sensor acting alone? (2) More important, given that a bulk filter and precision sensor are already in series, how much of an upgrade must be made to one key parameter to compensate for a decrement in another? What do the key trade-off curves look like?

The curves presented in this section were generated by using the synchronized firing threshold technique described in Appendix D. This technique is simply the firing rule based on the likelihood ratio (LLR) test that was shown to be optimal in Appendix C. The reader is referred to the appendices for further details.

### 4.1 PERFORMANCE ANALYSIS

Consider a modest bulk filter  $k_1 = 1$  and a precision sensor  $k_2 = 3$  with a relatively small traffic capacity  $T_2 = 3RV_0$ . The threat consisting of ten decoys per RV is given in normalized form by

$T_0 = (RV_0, 10 RV_0)$ . Throughout the remainder of the report the threat will remain the same, and so for simplicity the scale factor  $RV_0$  will be excluded, and a threat consisting of one RV and ten decoys will be considered.

Figure 11 shows leakage  $P_L$  as a function of inventory  $I$  for the bulk filter alone, the precision sensor alone, and the two in series. The curve for the precision sensor is similar to the one analyzed in Figure 4. Because its traffic capacity is so small here, the sensor is really only working at very low and very high values of  $I$ ; otherwise, discrimination is almost random. The bulk filter operating alone yields fair results provided the inventory is sufficiently high — 50 percent of the threat or greater. This percentage will generally be an unrealistically high inventory, namely, one interceptor for every two decoys.

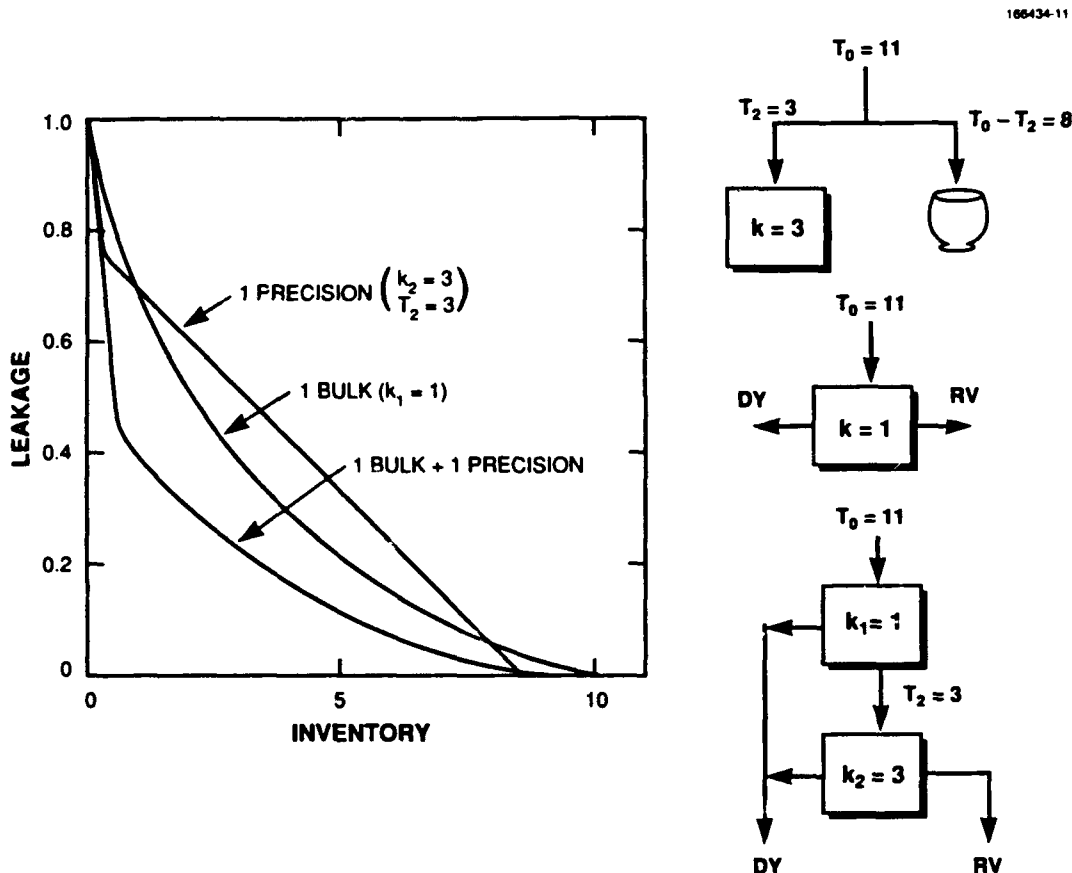


Figure 11. Performance of two sensors in series.

It is at inventories nominally sized to the non-offloaded payload  $1 RV_0 \leq I \leq 2 RV_0$  that the true effectiveness of the series arrangement shows itself. This region is where the two sensors optimally enhance one another. For an inventory of  $I = 1$ , which is less than 10 percent of the threat size, it is possible (with perfect interceptors) to kill 50 percent of the RVs.

Figure 12 shows sensor substitution performance. Given a bulk filter and a precision sensor in series, what happens if one of them is exchanged so that either two bulk filters or two precision sensors

are now both parallel? When two precision sensors are operating together, we assume that they are measuring disjoint sets of objects, so that, in effect, they operate as a single sensor with a traffic capacity of  $T_2 = 6$ . The two bulk filters, each with infinite traffic capacity, take independent measurements and achieve a joint k-factor of  $k = \sqrt{2}$ ; see Figure 7. In reality these two bulk filter measurements would probably be positively correlated thus degrading the overall quality [1].

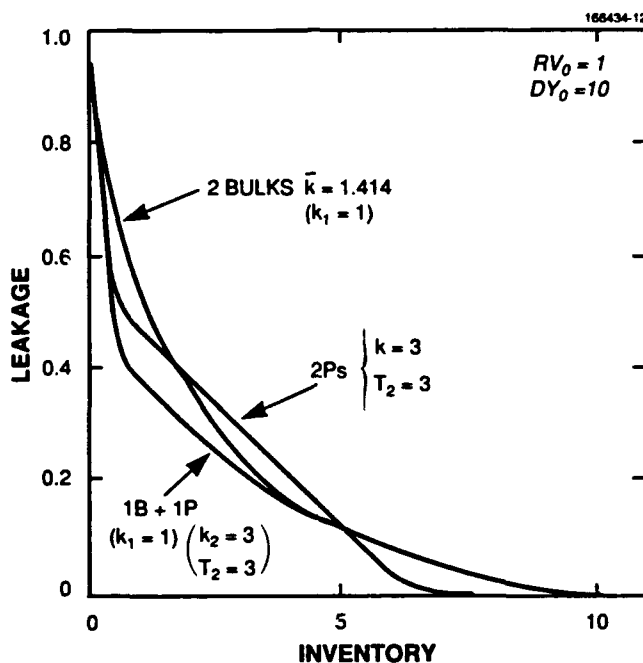


Figure 12. Sensor substitution performance.

Figure 12 shows that at inventories nominally sized to the non-offloaded payload, the bulk filter and precision sensor in series clearly dominate the other two candidate systems. However, at high inventories the two bulk filters are as good as the series network, and the two precision sensors are better than either of the others. These substitution problems are quite complex and clearly merit further study. In fact, the complexity of this problem will become more apparent when Figure 17, which trades off bulk filters for precision sensors, is examined.

#### 4.2 TRADE-OFF ANALYSIS

Trade-off analysis quantitatively demonstrates how much one key parameter must be upgraded to compensate for the decrement of another in order to keep system performance constant. The next five figures illustrate the trade-offs for the bulk filter and precision sensor in series.

Figures 13 and 14 illustrate the sensor quality trade-offs ( $k_1$  vs  $k_2$ ) for two separate cases: leakage held fixed and traffic capacity held fixed. In the first of these examples, Figure 13 shows  $k_1$  vs  $k_2$  with  $P_L$  fixed at 0.20 for three different levels of traffic capacity. For example, the curve corresponding to  $T_2 = 11$  shows all possible values that  $(k_1, k_2)$  can take on such that the system leakage stays at  $P_L = 0.20$  when the traffic capacity of sensor  $S_2$  is  $T_2 = 11$ . Because the total threat is  $T_0 = 11$ , this special case is where sensor  $S_2$  can

measure all of the objects — the full measurements' case. The locus of admissible  $(k_1, k_2)$  values is a circular arc satisfying  $(k_1^2 + k_2^2)^{1/2} = 2.85$ , which corresponds to Equation (1). When the traffic capacity is reduced, each curve develops a vertical asymptote. This asymptote is the minimum quality bulk filter required to achieve a leakage of  $P_L = 0.20$ . For a traffic capacity of  $T_2 = 6$ , a bulk filter with a k-factor of  $k_1 = 0.75$  or greater is needed. If the capacity of  $S_2$  is reduced to  $T_2 = 3$ ,  $k_1$  must be increased to  $k_1 = 1.5$  or greater. For sufficiently high values of traffic capacity, around  $T_2 \approx 8.8$ ,  $P_L = 0.20$  can be achieved with a perfect ( $k_2 = \infty$ ) precision sensor alone (i.e.,  $k_1 = 0$ ); however, for smaller (in the sense of  $T_2$ ) precision sensors, a bulk filter is always necessary. All of the curves coalesce into one as  $k_2$  goes to zero, which occurs at the point where the bulk filter is just good enough to carry out all of the necessary discrimination.

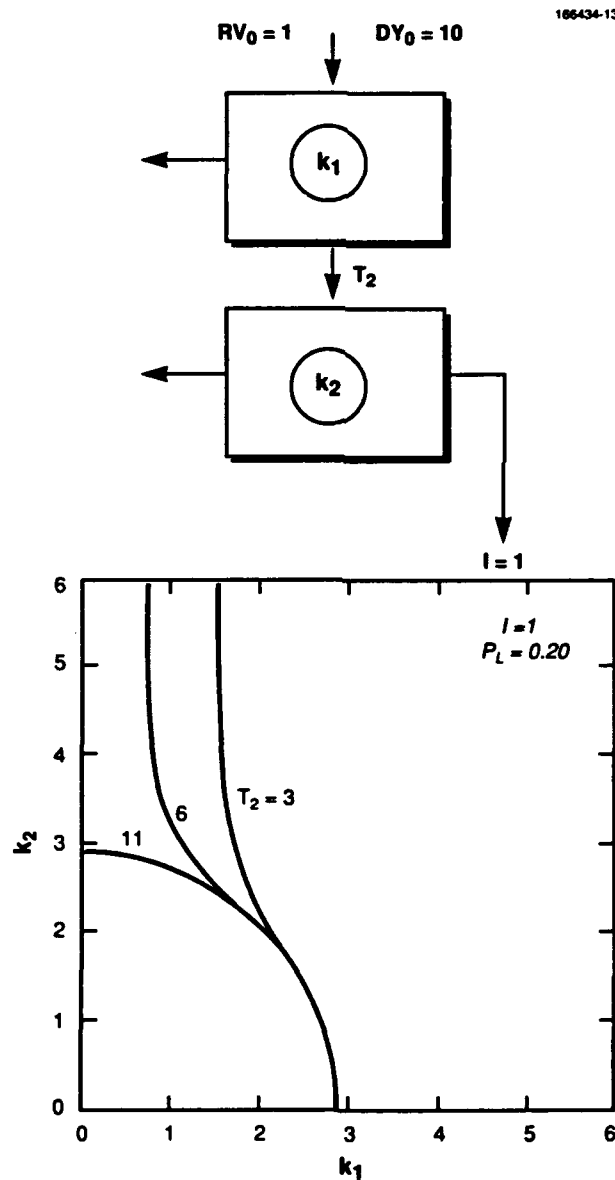


Figure 13. Sensor quality trade-off: leakage fixed.

Figure 14 shows a sensor quality trade-off ( $k_1$  vs  $k_2$ ) for  $T_2 = 3$  fixed, for three possible leakages. That is, given a fixed traffic capacity for sensor  $S_2$ , what are the admissible ( $k_1, k_2$ ) values required to achieve different leakages? For leakages less than about  $P_L = 0.66$ , the figure shows that a bulk filter is needed because the curves asymptote vertically as  $k_1$  decreases. As on the previous figure, these vertical asymptotes correspond to a perfect precision sensor, which means that all leakage is due to the bulk filter alone. The asymptotic values of  $k_1$  represent the minimum quality required.

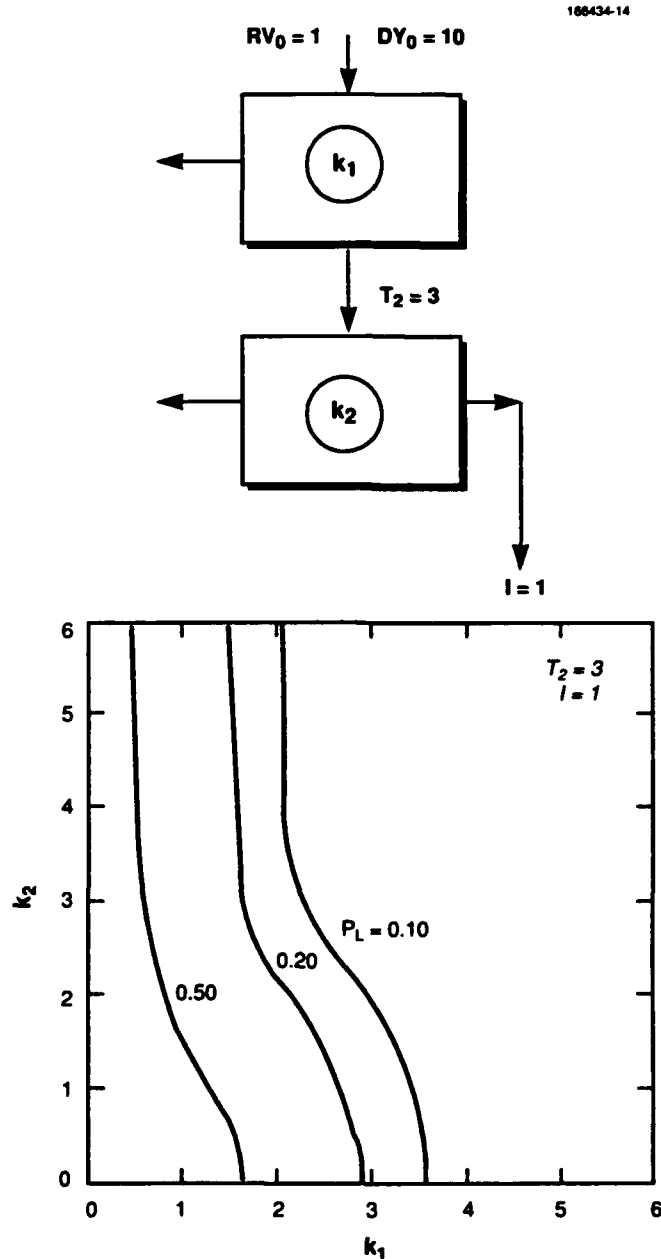


Figure 14. Sensor quality trade-off: traffic fixed.

Figure 15 shows a sensor  $S_2$  trade-off ( $T_2$  vs  $k_2$ ) for curves of constant leakage. Here, the quality of the bulk filter is fixed at  $k_1 = 1$ , and the trade-off between size  $T_2$  and accuracy  $k_2$  of the precision sensor is examined. What is most striking about this set of curves is the very narrow operating region delineated by the pair of dashed lines. The dashed lines enclose what is known as the knee of the curve for the family shown here. This region is where a change in one of the parameters (e.g.,  $\Delta k_2$ ) yields a concomitant change in the other — a quid pro quo. The remainder of the trade-off curves are so steep or so flat that a change in the sensitive parameter requires a disproportionately large change in the other to maintain the fixed leakage. A system design is most stable when parameters are chosen inside the operating region whenever possible.

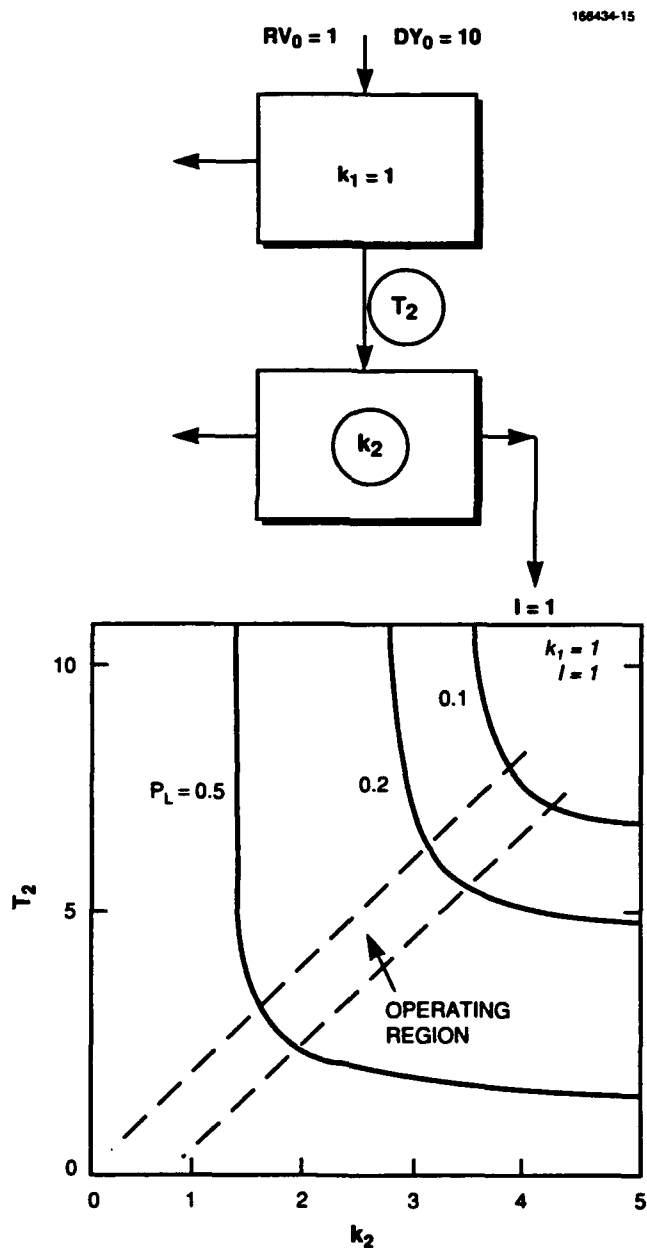


Figure 15. Precision sensor trade-off.

It should not be surprising that the curves asymptote so flatly or steeply. For  $k_1 = 1$ , to achieve the relatively small leakages shown here, a minimum  $k_2$  is required even if the second sensor has infinite traffic capacity. In fact, for a given leakage (e.g.,  $P_L = 0.20$ ) one can look at Figure 3(a) to see that for  $I = 1$ , an overall k-factor of almost 3.0 is required. This situation would imply that sensor  $S_2$  requires a k-factor given by  $k_2 = (k^2 - k_1^2)^{1/2} = \sqrt{8}$ , which is approximately the value at the intersection at the top of the graph along the  $T_2 = 11$  line.

What is more interesting is that no matter how good the sensor is, a certain minimum traffic capacity is required. The flattening out of these curves shows that there is a hard lower limit to the size of the precision sensor in a series. Referring to Figure 9, the traffic capacity  $T_2$  determines the location of the traffic threshold  $\tau$ . If the number of RVs, with an  $x_1$  discriminant less than  $\tau$ , exceeds the leakage requirement, then achieving the required overall leakage will be difficult. It may still be possible if there are enough interceptors because of the synchronized threshold firing rule. But in general — and certainly for the inventory level of  $I = 1$  in this example — the leakage due to a traffic threshold that is set too high cannot be overcome.

The next set of curves illustrates the inventory/traffic capacity trade-off ( $I$  vs  $T_2$ ). Figure 16 shows curves of constant leakage ( $T_2, I$ ) are varied with the sensor quality of both sensors fixed at  $k_1 = 1$  and  $k_2 = 3$ . As the curves show, one can always compensate for lack of traffic capacity with more interceptors. (Because we are using hypothetically perfect interceptors here to demonstrate discrimination leakage, zero leakage can be achieved with  $I = 11$  interceptors, even when no sensors are present.) Also, the vertical asymptotes again yield hard lower limits on the minimum number of interceptors required to achieve these leakages. The other very important quality here is the operating region of each of these curves, which is large and almost linear.

The operating regions consist of those portions of the curves below the dashed line. The size and linearity have two ramifications. One pertains to performance alone: a large amount of discretion is left to the discrimination architect in trading guns for sensors. Also, over this large regime there is an almost constant marginal rate of exchange (the slope of the curve). Linearity is a double-edged sword. The other ramification shows up if linear cost curves are overlaid on top of the trade-off curves (i.e., cost curves of the form  $\alpha I + \beta T_2 = \text{constant}$ , where  $\alpha$  and  $\beta$  represent unit cost of an interceptor or a precision sensor). This sort of analysis will not be developed here because it lies outside the scope of this report, but we must mention that the linearity of the trade-off curves leads to instabilities with discontinuous jumps in optimal apportionment if minimum cost becomes the sole design criterion.

Figure 17 shows bulk filter/precision sensor trade-offs. As discussed in Section 4.1, adding bulk filters is equivalent to increasing  $k_1$  according to the root-sum-square rule; the  $k_1$  axis is a measure of the number of bulk filters forming sensor  $S_1$ . Adding precision sensors is equivalent to increasing  $T_2$  (up to  $T_2 = 11$ , provided each sensor measures different subsets of objects with little or no overlap). So the  $T_2$  axis is a measure of the number of precision sensors forming sensor  $S_2$ .

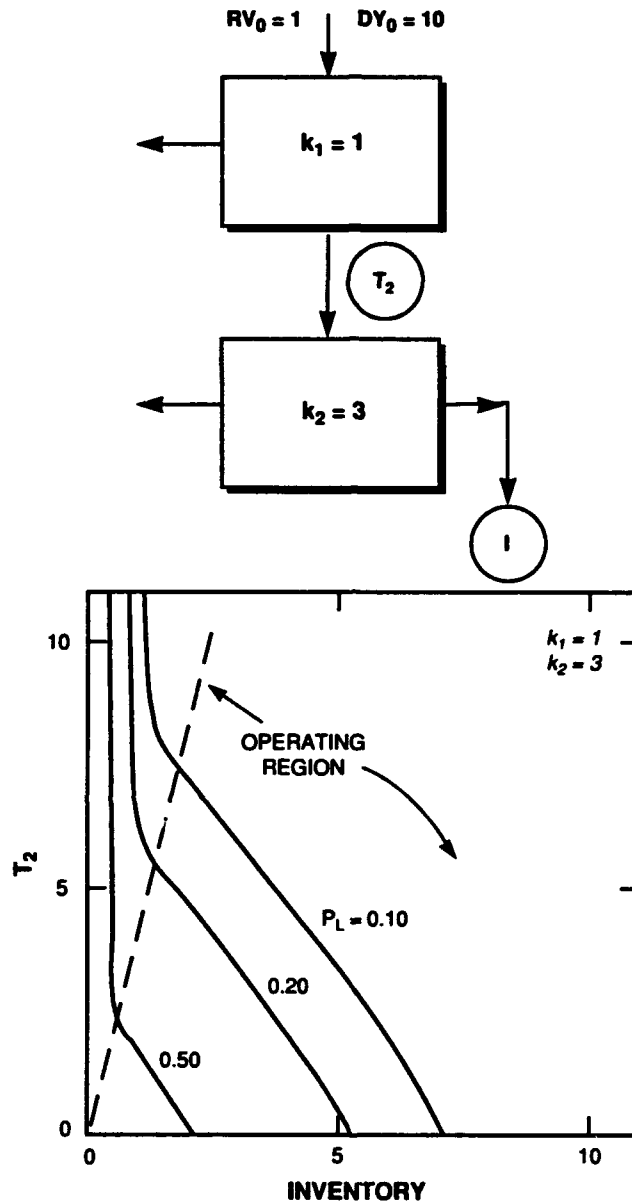


Figure 16. Traffic/inventory trade-off.

Trade-off curves for three values of leakage are shown with fixed parameters  $k_2 = 3$  and  $l = 1$ . There are no clear messages here. For sufficiently high values of  $k_1$ , no precision sensor is needed because the bulk filter approaches it in quality. For very low leakages (e.g.,  $P_L = 0.10$ ), a minimum  $k_1$  is required because  $k_2 = 3$  is inadequate even with no traffic limit, otherwise sufficient traffic capacity can achieve the required performance. Two of the curves have sharp knees; one is almost linear. In fact, the middle curve can best be described as having a trick knee and a sway back. When the inventory level is increased, other more complex interactions are unleashed; they are not shown here. The basic message

here is that the trade-off between the amount of resources that one should put into bulk filters and take out of precision sensors (or vice versa), based on a leakage performance criteria alone, is very complex. Adding cost as a criterion permits selection of an operating point, but this point is very sensitive to the various cost ratios. The reader is invited to draw some families of linear cost lines on the figure using different slopes and observe how the various optima change. As mentioned at the end of Section 4.1, this is an area that requires further work.

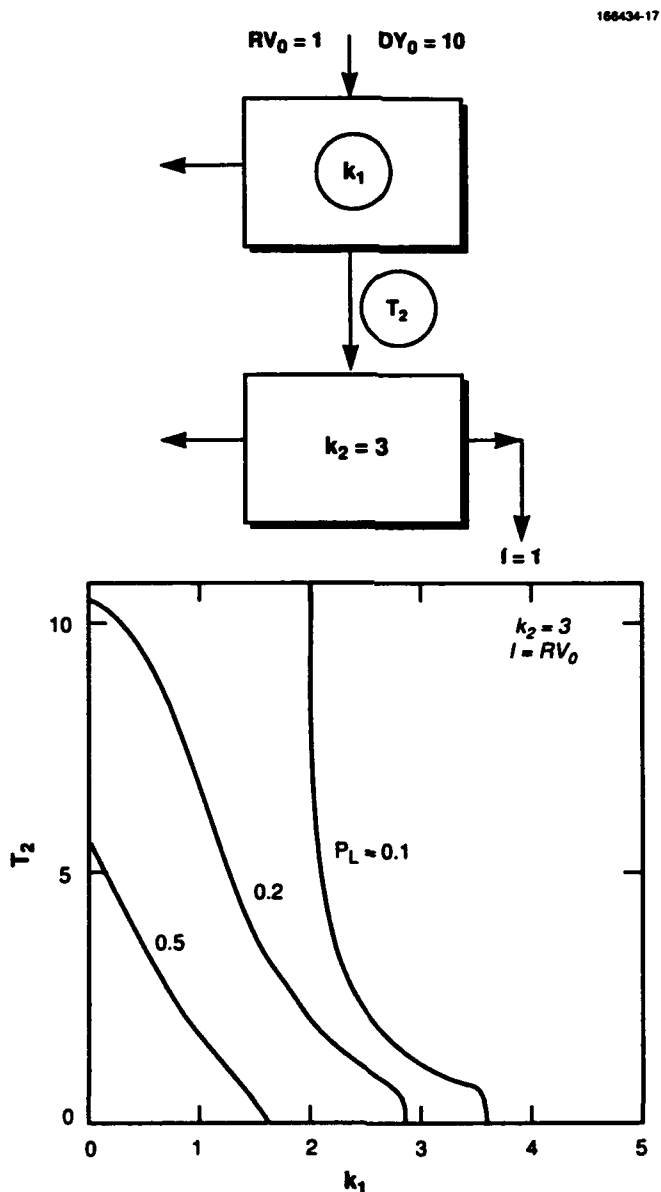


Figure 17. Bulk filter/precision sensor trade-off.

## 5. SUMMARY

The problem of improving the performance of a sensor with limited traffic capacity by forming a series network has been addressed. In the process, groundwork has been laid down for the analysis of arbitrary sensor networks to be completed in future reports. The performance of a single sensor was modeled in a general context independent of engineering constructs. Such a sensor's performance has been compared with that of one with a fixed traffic limit. After quantifying the loss of performance with the loss in traffic capacity, a proposal to remedy the situation was made that linked together a bulk filter with the traffic-limited sensor — now denoted as a precision sensor. Finally, the performance and trade-off characteristics of the two sensors in series were studied.

Some general summary points follow.

1. This report introduces a new methodology to analyze the performance of multiple sensor networks. Along with related results in the references given on parallel networks and forthcoming results on series networks of arbitrary length, the tools to analyze sensor arrangements of any network topology will become available.
2. For series models, traffic capacity is an important sensor parameter with significant effects on network performance. In the past, its effects were poorly understood because of a lack of theoretical models. This problem has now been remedied for the two-sensor arrangement.
3. For traffic-limited sensors or two sensors in series, there is no single measure of quality such as the k-factor. The entire leakage performance curve must be retained.

Some specific points of interest follow.

1. Low-quality sensors degrade slowly with traffic and are best used as bulk filters. High-quality sensors tend to degrade faster and are therefore more suited for traffic-limited precision sensors.
2. When combining two classes of sensors, either bulk and/or traffic-limited precision, the bulk and precision in series perform best for moderate interceptor inventories.
3. When traffic capacity is limited and inventories are nominal, a bulk filter is always required to achieve small leakages. There are hard lower limits on the quality  $k_1$  of the bulk filter that is required. There are always hard lower limits on the inventory required. (Hard lower limits show up on trade-off curves as vertical or horizontal asymptotes.)
4. The precision sensor in the series arrangement has hard lower limits on both sensor quality  $k_2$  and traffic capacity  $T_2$ . The precision sensor trade-off curves have what is known as sharp knees that indicate a narrow operating region in a well-designed architecture.

## APPENDIX A

### A COMPARISON OF TRAFFIC-LIMITED AND CONTINUOUSLY DEGRADED SENSORS

In this appendix a brief but pertinent discussion is presented of alternative models for a single sensor with traffic degradation. The traffic-limited sensor is a limiting case of the more general situation presented here.

The most common alternative to the traffic-limited sensor is a sensor with continuous degradation where the performance of the sensor, as measured by an "effective" k-factor  $k_e$ , is given by

$$k_e = k(T_1, T) = k / \left[ 1 + k^2 \max(0, T - T_1) / T_1 \right]^{1/2} \quad (\text{A.1})$$

and is plotted in Figure A-1. The figure shows that if the actual traffic  $T$  presented to the sensor exceeds a critical value  $T_1$ , then the nominal k-factor  $k$  will decrease according to the factor in the brackets in Equation (A.1). For traffic levels below  $T_1$ , no degradation is seen in the k-factor. Note that the  $k_e$  in Figure A-1 applies to all 11 targets and not just those beyond the critical value  $T_1$ .

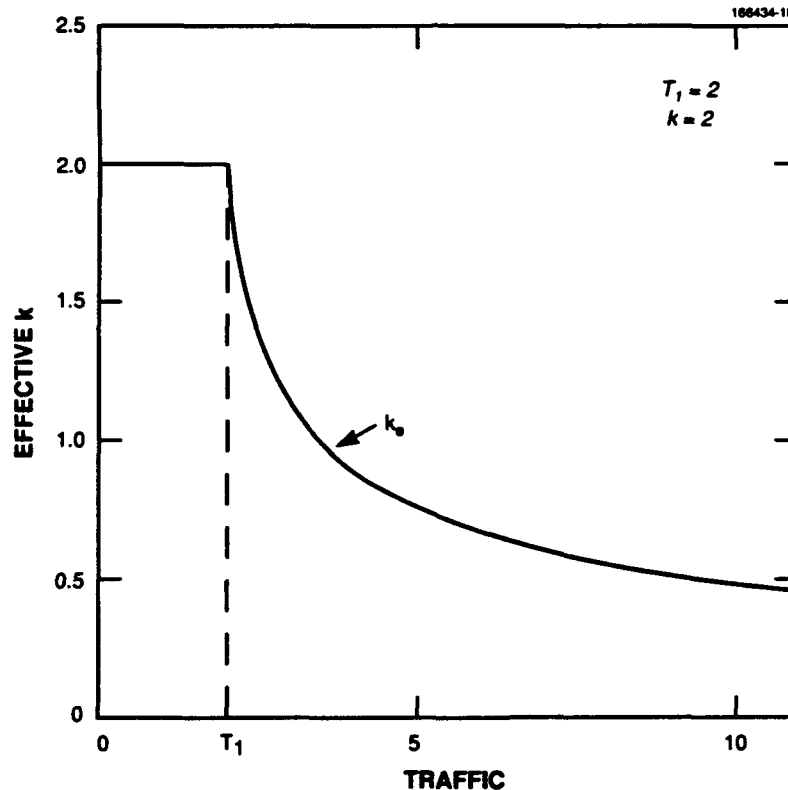


Figure A-1. Continuous degradation traffic model.

Equation (A.1) can be derived based on various uniform measurement strategies where the measurement uncertainty depends on the number of pulses (or length of time) that a sensor can devote to each target object. Such strategies are discussed elsewhere [1]. Equivalently, one could consider that Equation (A.1) is simply a reasonable ad hoc rule for sensor degradation. If so, then it is also reasonable to compare such a rule to the traffic-limited model. In the traffic-limited model,  $T_1$  is the maximum amount of traffic that the sensor can handle (its limit); traffic above this limit is subject to random discrimination. The two models are compared by looking at sensor performance plotted as leakage vs interceptor inventory using the usual threat,  $T_0 = 1 RV + 10 DY$ . The critical traffic value  $T_1$  in the continuous case or limit in the traffic-limited case is the adjusted parameter in each of these figures. (From now on, we shall call  $T_1$  the traffic capacity of the sensor, regardless of whether it is traffic limited or of the continuous degradation type; the context, if necessary, will always be clear.) Figure A-2 contains two sets of working curves for a nominal k-factor of  $k = 2$  and traffic capacities  $T_1 = 1, \dots, 11$ . Clearly, for either case  $T_1 = 11$  represents no degradation whatsoever and is the usual performance curve for  $k = 2$ . The curves for the traffic-limited sensor are obtained precisely in the manner discussed in Section 2. The curves for the continuous case are ordinary performance curves for a reduced effective k-factor  $k(T_1, T)$  given by Equation (A.1) with  $T$  fixed at  $T_0 = 11$ , the actual threat.

Using similar working curves for nominal  $k = 1, 2$ , and  $3$ , a comparison can be made of the two kinds of sensors to see which one gives a better performance. These comparisons are shown in Figure A-3. The two capacities  $T_1 = 2$  and  $5$  were selected because they are very close to the crossover values indicated on the lower right part of the figure. For  $k = 1$  the continuous model dominates the traffic-limited model in the sense that its leakage curve is lower along almost the entire inventory axis. As  $k$  increases, the traffic-limited model begins to dominate at increasingly lower traffic capacities. The implications are (1) bulk filters (with low nominal  $k$ ) perform better by measuring every object and accepting the decreased effective  $k$  and (2) precision sensors (with high nominal  $k$ ) give better performance with fixed traffic limits.

A point should be stressed here. Traffic-limited sensors have not been investigated in this report simply because of the result above. Rather, some sensors, because they require a minimum measurement time per object, must necessarily act as traffic-limited sensors. The result above confirms that they are behaving efficiently if their k-factor is sufficiently high, based on the model for k-factor degradation given by Equation (A.1). Finally, and most important, for low inventory/threat ratios, the traffic-limited sensor is clearly superior to the continuous degradation model. The improvement is substantial for all values of  $k \geq 1$ .

Two extreme cases of traffic degradation have been explored: (1) continuous degradation where the entire threat  $T_0$  is presented to the sensor and  $k_e = k(T_1, T_0)$  and (2) the traffic-limited case where the sensor looks at nothing beyond its traffic capacity  $T_1$  and  $k_e = k(T_1, T_1) = k$ . However, Equation (A.1) is a reasonable model for traffic degradation for any effective level of traffic  $T_e$  presented to the sensor, where  $T_1 \leq T_e \leq T_0$ . In this case, the sensor looks at  $T_e$  objects with an effective k-factor given by  $k_e = k(T_1, T_e)$  from Equation (A.1), and the remaining  $T_0 - T_e$  objects are discriminated randomly. If  $T_e = T_1$ , the traffic-limited case applies, and if  $T_e = T_0$ , the continuous case applies. Figure A-4 shows a nomogram constructed from Equation (A.1) using values of traffic capacity  $T_1 = 1, \dots, 11$  for our usual threat  $T_0 = 1 RV + 10 DY$ .

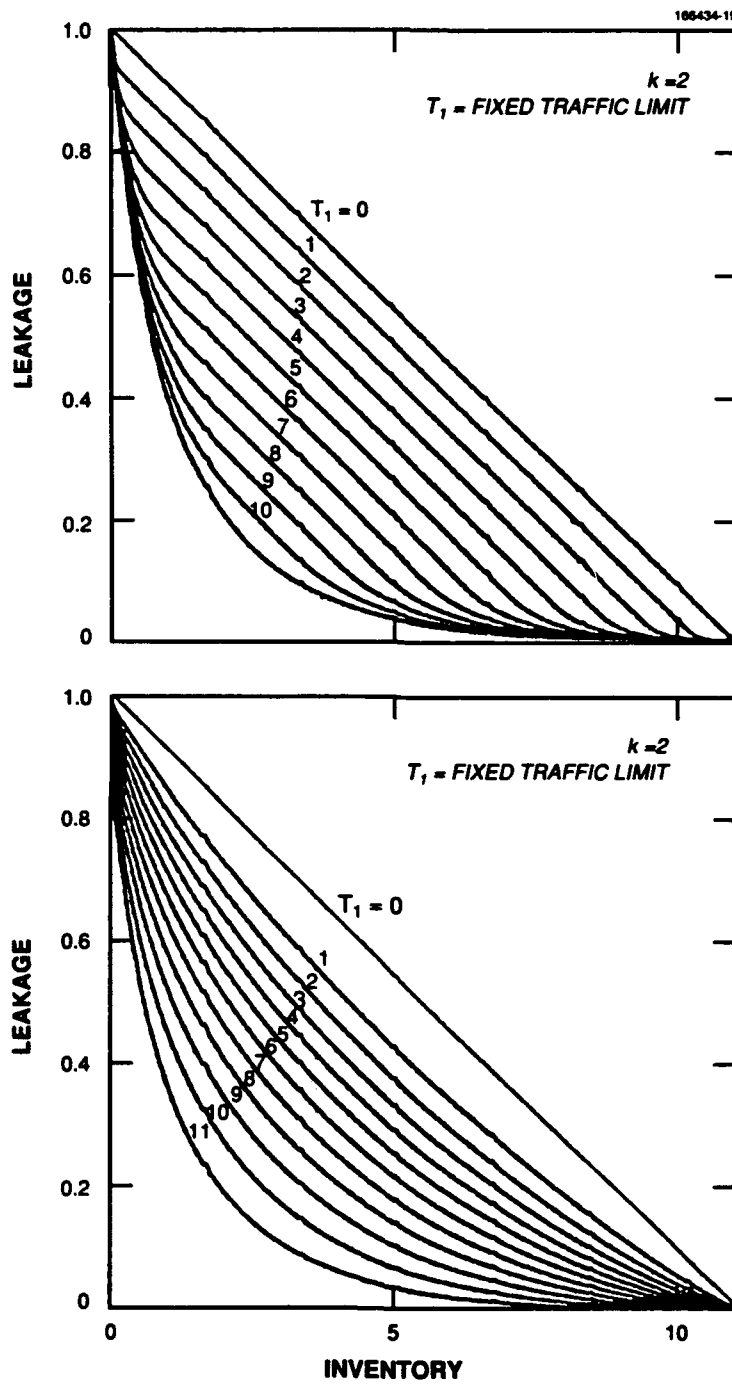
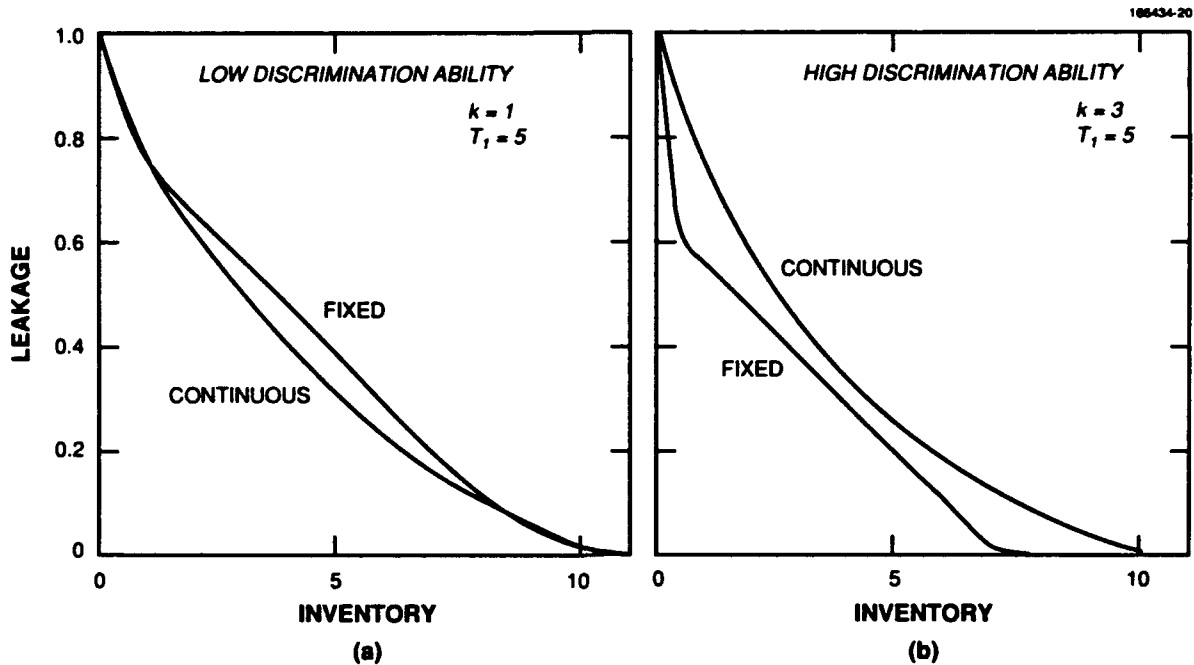


Figure A-2. Performance curves for fixed limit and continuous models.



	BEST AT LOW $T_1$	CROSSOVER VALUE	BEST AT HIGH $T_1$
$k = 1$	CONTINUOUS	$T_1 = 11$	CONTINUOUS
$k = 2$	CONTINUOUS	$T_1 = 5$	FIXED LIMIT
$k = 3$	CONTINUOUS	$T_1 = 2$	FIXED LIMIT

Figure A-3. Comparison of fixed limit and continuous models.

The nomogram may be used in various ways. The first is simply the straightforward application of Equation (A.1). The bottom of Figure A-4 shows the case of a sensor with capacity  $T_1 = 2$  observing the portion  $T_c = 8$  of the threat. The box indicates that all  $T_c$  of these objects are discriminated with an effective  $k$ -factor of  $k_c = 0.50 k$ , where  $k$  is the unstressed nominal  $k$ . The remaining  $T_0 - T_c$  objects are discriminated randomly.

Another application concerns sensor coverage. Suppose that  $M$  sensors, each with traffic capacity normalized to  $T_1 = 1$ , have a nominal  $k$ -factor equal to  $k$ . Suppose it is desired to measure a threat of size  $T_c = 10 T_1$ , for example, and maintain a discrimination quality of  $k_c = 0.7 k$ . Then, locating the appropriate point, indicated by a large dot on the bottom figure, we see that approximately  $5M$  sensors are

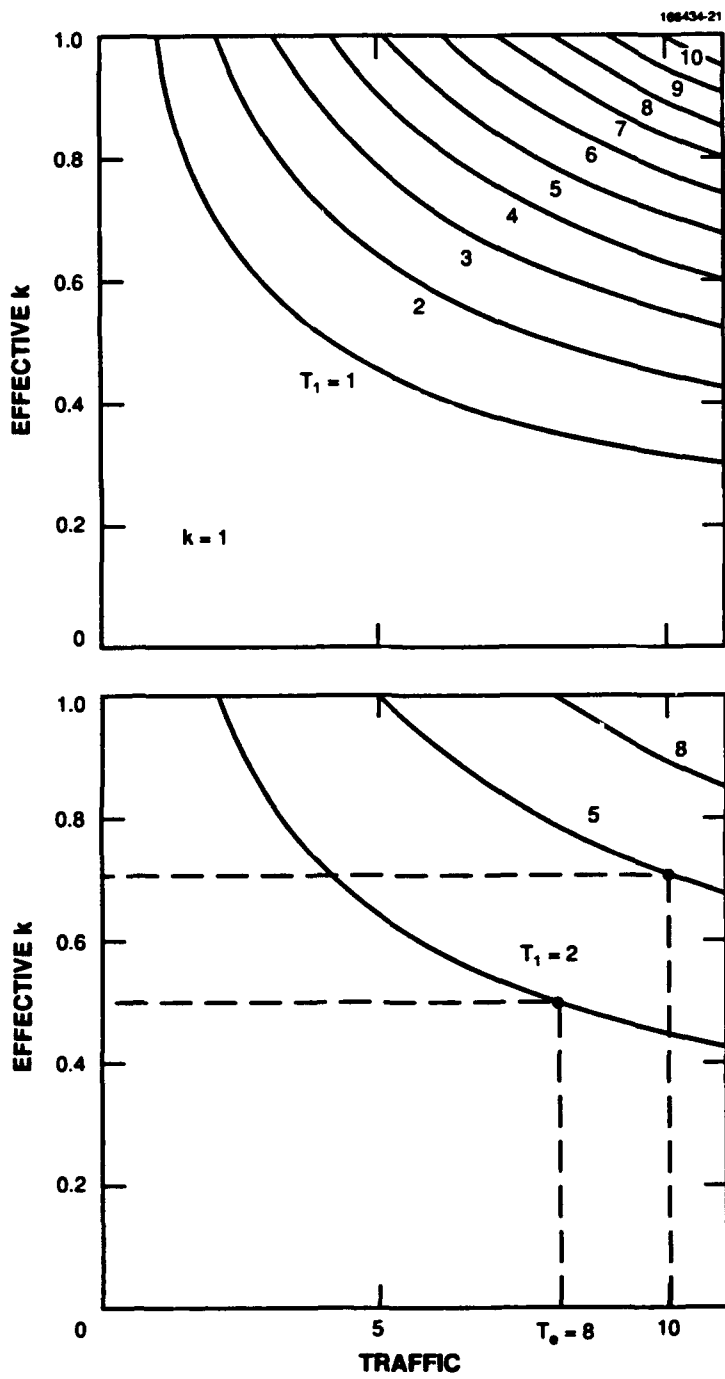


Figure A-4. Generalized-continuous model.

required for coverage (or equivalently,  $M$  sensors with capacity  $T_1 = 5$ ). This number,  $5M$ , is the absolute minimum that the defense requires. To achieve this requirement, nearly perfect coordination of measurement is necessary; that is, there must be virtually no overlap between the subsets of objects that each sensor measures. Clearly, most of the important issues concerning sensor coverage have been left out here; this example serves only to give a quick ballpark estimate in a highly idealized homogeneous battle space.

In Figure A-3 the two limiting cases, continuous degradation or traffic limited, were examined to determine which one yielded the lower leakage, and it was found that it depends upon the nominal  $k$ -factor and traffic capacity of the sensor and upon the interceptor inventory. Here, we examine briefly whether some intermediate value of effective traffic  $T_1 \leq T_e \leq T_0$  is the optimal level to direct to the sensor; the remaining traffic  $T_0 - T_e$  will be discriminated randomly. Figure A-5 shows the result of a numerical investigation. Here, the traffic capacity is fixed at  $T_1 = 2$ , and effective traffic varies continuously on the interval  $[T_1, T_0]$ . Ten different levels of inventory parameterize these leakage curves. For each curve the global minimum is indicated by a black dot as a visual aid. To help orient the reader (1) the set of all left-hand endpoints represent the traffic-limited case  $T_e = T_1$  and form a discretized version of curve (a) in Figure A-3(b), while (2) the set of all right-hand endpoints represent the continuous degradation case  $T_e = T_0$  and form curve (b) in Figure A-3(b).

A precise analytical location of the global minima is beyond the scope of this report at present. Generally, one of the two limited cases yields the minimum. For the cases where an internal minimum occurs (e.g.,  $I = 2, 8, \text{ or } 9$ ), it appears that not much accuracy (in leakage) is lost by choosing the best limiting case. We feel that the optimal level of effective traffic  $T_e$  can best be understood by looking at optimal measurement strategies as discussed in Holmes and Rocklin [1].

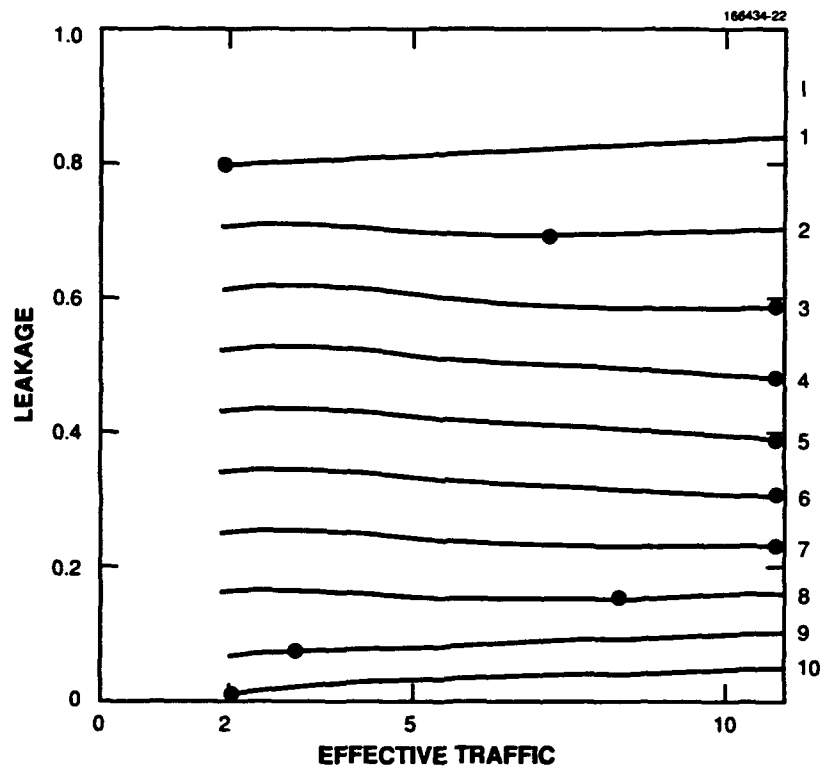


Figure A-5. Performance of generalized-continuous model

## APPENDIX B

### DERIVATION OF THE BASIC DENSITY FUNCTION FOR A CHAIN OF SENSORS IN SERIES

In this appendix a density function is presented for the classification of an object by all  $n$  sensors in a series arrangement. We will derive the density function for three sensors in series — the extension to  $n$  sensors will then be straightforward. The advantages of having a density function are many. For example, we might desire certain conditional probabilities. What is the probability that an object will be classified as an RV given that earlier sensors in the chain yielded a particular vector of measurements? Another use is computational. For example, numerical routines exist for evaluating multiple integrals over rectangular regions. For judiciously chosen limits of integration, such a routine, coupled with the density function derived here, will yield the probability that an object remains unclassified by all sensors in the chain.

Consider three sensors in series. We shall be interested in such probabilities as

Pr {all three sensors declare object uncertain} .

If these three sensors were the first three sensors in a chain, this arrangement would represent the fraction of all the objects that continue on for more measurements. The particular probability is given by

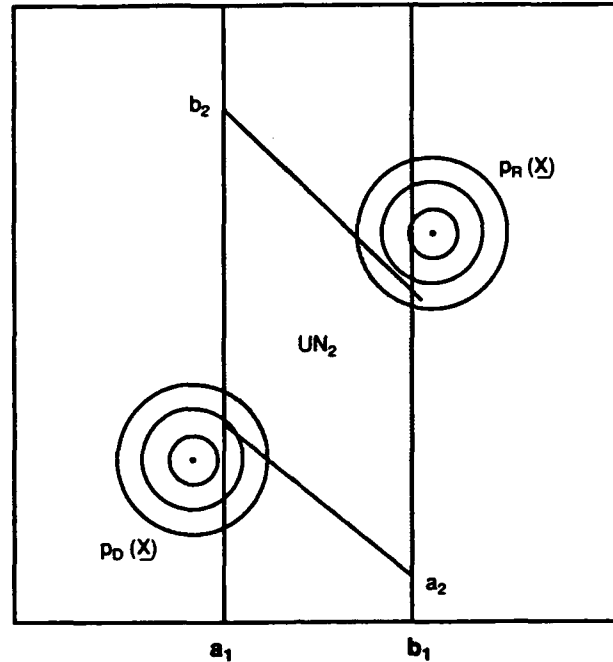
$$\begin{aligned} & \text{Pr \{all three sensors declare object uncertain\}} \\ & = \text{Pr} \left\{ a_3 < Y_1 + Y_2 + Y_3 < b_3, a_2 < Y_1 + Y_2 < b_2, a_1 < Y_1 < b_1 \right\} , \end{aligned} \quad (\text{B.1})$$

where  $Y_1$ ,  $Y_2$ , and  $Y_3$  are the log-likelihood functions of the measurements of sensors  $S_1$ ,  $S_2$ , and  $S_3$ , respectively. The pairs  $(a_i, b_i)$  represent the values of the decision thresholds for each sensor  $S_i$ . In what follows,  $a_i$  and  $b_i$  need not have such an interpretation; they are simply arbitrary values. Figure B-1 shows the region defined by Equation (B.1) for two sensors. For three or more sensors, the region is a paralleloprism in higher dimensions. For convenience, the random variables  $Y_1$ ,  $Y_2$ , and  $Y_3$  are called the measurement variables. The individual probability distribution and density functions of the measurement variables are denoted by

$$\begin{aligned} Y_1: & F(y_1), f(y_1) , \\ Y_2: & G(y_2), g(y_2) , \text{ and} \\ Y_3: & H(y_3), h(y_3) . \end{aligned}$$

Because classifications are based on linear sums of the measurement variables, the following decision variables are defined by

$$\begin{aligned} Z_1 &= Y_1 , \\ Z_2 &= Y_1 + Y_2 , \text{ and} \\ Z_3 &= Y_1 + Y_2 + Y_3 . \end{aligned}$$



$UN_2$  = REGION WHERE BOTH SENSORS DECLARE AN OBJECT UNCERTAIN

Figure B-1. Region of feature space passed on to sensor  $S_3$ .

Thus, the probability that all three sensors declare an object uncertain is given in terms of the decision variables as

$$\Pr \{ a_3 < Z_3 < b_3, a_2 < Z_2 < b_2, a_1 < Z_1 < b_1 \} .$$

Of particular interest is the joint distribution function and density function of the decision variables

$$P(h_1, h_2, h_3) = \Pr \{ Z_3 < h_3, Z_2 < h_2, Z_1 < h_1 \} \quad \begin{array}{l} h_1 = z_1 \\ \text{at } h_2 = z_2 \\ h_3 = z_3 \end{array} .$$

and

$$p(z_1, z_2, z_3) = \partial^3 P(h_1, h_2, h_3) / \partial h_1 \partial h_2 \partial h_3 \quad \begin{array}{l} h_1 = z_1 \\ \text{at } h_2 = z_2 \\ h_3 = z_3 \end{array} .$$

The joint density function  $p(z_1, z_2, z_3)$  will be derived using conditional densities and the relation

$$p(z_1, z_2, z_3) = p(z_3 | z_2, z_1) p(z_2 | z_1) p(z_1) .$$

The conditional distribution of  $Z_3$  given values for the other decision variables is given by

$$\begin{aligned}
 P(Z_3 < b_3 | Z_2 = z_2, Z_1 = z_1) \\
 &= P(Y_1 + Y_2 + Y_3 < b_3 | Y_1 + Y_2 = y_1 + y_2, Y_1 = y_1) \\
 &= P[Y_3 < b_3 - (y_1 + y_2)] \\
 &= H[b_3 - (y_1 + y_2)] \\
 &= H(b_3 - z_2) .
 \end{aligned}$$

Consequently,

$$\begin{aligned}
 p(z_3 | z_2, z_1) &= \partial H(b_3 - z_2) / \partial b_3 \text{ at } b_3 = z_3 \\
 &= h(z_3 - z_2) .
 \end{aligned} \tag{B.2}$$

Similarly,

$$\begin{aligned}
 P(Z_2 < b_2 | Z_1 = z_1) &= P(Y_1 + Y_2 < b_2 | Y_1 = y_1) \\
 &= P(Y_2 < b_2 - y_1) \\
 &= G(b_2 - y_1) ,
 \end{aligned}$$

and

$$p(z_2 | z_1) = g(z_2 - z_1) . \tag{B.3}$$

Using Equations (B.2) and (B.3) and the equality of densities  $p(z_1) = f(z_1)$ , the additional conditional and joint density functions are obtained.

$$\begin{aligned}
 p(z_2, z_3 | z_1) &= h(z_3 - z_2) g(z_2 - z_1) , \\
 p(z_1, z_2) &= g(z_2 - z_1) f(z_1) ,
 \end{aligned}$$

and finally,

$$p(z_1, z_2, z_3) = h(z_3 - z_2) g(z_2 - z_1) f(z_1) . \tag{B.4}$$

Equation (B.4) is our required joint density function. The probability that all three sensors classify an object as uncertain can now be calculated.

$$\begin{aligned} & \Pr \left\{ a_3 < Y_1 + Y_2 + Y_3 < h_3, a_2 < Y_1 + Y_2 < h_2, a_1 < Y_1 < h_1 \right\} \\ &= \int_{a_1}^{h_1} \left[ \int_{a_2}^{h_2} \left[ \int_{a_3}^{h_3} p(u, v, w) dw \right] dv \right] du \\ &= \int_{a_1}^{h_1} \left[ \int_{a_2}^{h_2} \left[ \int_{a_3}^{h_3} h(w-v) g(v-u) f(u) dw \right] dv \right] du \end{aligned}$$

This is a multiple integral over a rectangular region. Useful conditional probabilities can also be calculated. For example, what is the conditional probability that sensor  $S_3$  will classify an object as a  $DY$  for a threshold set at  $\eta$  given that the previous two sensors declared the object uncertain?

$$\begin{aligned} & \Pr \left\{ Y_1 + Y_2 + Y_3 < \eta \mid a_2 < Y_1 + Y_2 < h_2, a_1 < Y_1 < h_1 \right\} \\ &= \int_{a_1}^{h_1} \int_{a_2}^{h_2} H(\eta - v) g(v - u) f(u) dv du / \int_{a_1}^{h_1} \int_{a_2}^{h_2} g(v - u) f(u) dv du \end{aligned}$$

Finally, the generalization to  $n$  sensors in series is straightforward. If  $Y_i$  represents the  $i$ th measurement variable with density and distribution functions  $f_i(y_i)$  and  $F_i(y_i)$  and the decision variables  $Z_i$  are defined by

$$\begin{aligned} Z_1 &= Y_1 \\ Z_2 &= Y_1 + Y_2 \\ &\vdots \\ Z_j &= Y_1 + Y_2 + \dots + Y_j \end{aligned}$$

then the joint density function for all  $n$  decision variables is given by

$$p(z_1, z_2, \dots, z_n) = f_n(z_n - z_{n-1}) f_{n-1}(z_{n-1} - z_{n-2}) \dots f_2(z_2 - z_1) f_1(z_1)$$

## APPENDIX C

### LOG-LIKELIHOOD RATIO AS A DECISION FUNCTION

Let  $p_R(x)$  and  $p_D(x)$  be the RV and DY density functions defined on the Euclidean space  $R^N$ . They may be discontinuous. Let  $\Omega_R$  and  $\Omega_D = R^N - \Omega_R$  be subsets of  $R^N$  such that  $x \in \Omega_R$  means classify an object as an RV, and  $x \in \Omega_D$  means classify an object as a decoy. Consider the following leakage/inventory cost function:

$$\begin{aligned}
 J &= P_L + \mu I \quad . \\
 J &= \int_{\Omega_D} p_R(x) dx + \mu \left[ RV \int_{\Omega_R} p_R(x) dx + DY \int_{\Omega_R} p_D(x) dx \right] \\
 &= P_L + \mu RV (1 - P_L) + \mu DY P_F \\
 &= \mu RV + P_L (1 - \mu RV) + \mu DY P_F \quad .
 \end{aligned}$$

The cost is now in the form of a constant  $\mu RV$  and the two error integrals

$$\begin{aligned}
 P_L &= \int_{\Omega_D} p_R(x) dx \quad , \text{ and} \\
 P_F &= \int_{\Omega_R} p_D(x) dx \quad .
 \end{aligned}$$

We will now show that the boundary of the decision region  $\Omega_R$ ,  $\partial\Omega_R$  is such that the likelihood ratio  $\Lambda(x)$  is a constant on  $\partial\Omega_R$ . Thus, a constant  $\lambda$  exists such that

$$\Omega_R = \{x: \Lambda(x) \geq \lambda\} \quad .$$

This relation will be shown to be true regardless of the location and nature of the discontinuity of the surfaces of the two densities (as long as there are no  $\delta$ -functions, i.e., no probability masses). The argument below is independent of any discontinuity surfaces because they form a set of measure zero with respect to the various integrals.

The proof is straightforward. Let  $J^*$  be the cost using the decision region  $\Omega_{*R}$  defined above ( $\Omega_{*R} = \{x: \Lambda(x) \geq \lambda^*\}$ ) for some appropriate  $\lambda^*$ . Let  $J$  be cost associated with any other decision region  $\Omega_R$  defined by some other decision rule. Figure C-1 shows a schematic representation of these regions and their complements. The difference in cost using these two sets of decision rules is given by

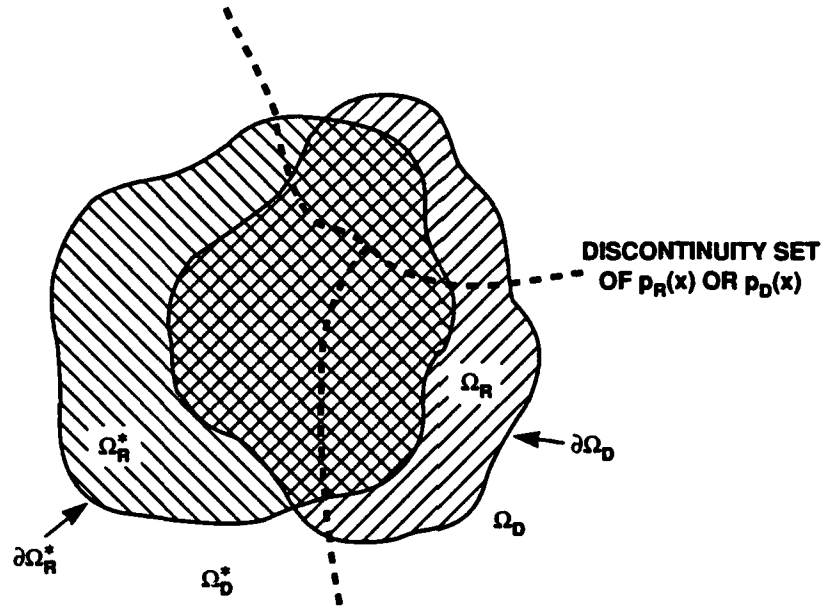


Figure C-1. Optimal and nonoptimal decision regions.

$$\begin{aligned}
 J - J^* &= \mu RV + (1 - \mu RV) \int_{\Omega_D} p_R(x) dx + \mu DY \int_{\Omega_R} p_D(x) dx \\
 &\quad - \left[ \mu RV + (1 - \mu RV) \int_{\Omega_{*D}} p_R(x) dx + \mu DY \int_{\Omega_{*R}} p_D(x) dx \right] \\
 &= (1 - \mu RV) \left[ \int_{\Omega_D} p_R(x) dx - \int_{\Omega_{*D}} p_R(x) dx \right] + \mu DY \left[ \int_{\Omega_R} p_D(x) dx - \int_{\Omega_{*R}} p_D(x) dx \right] \\
 &= (1 - \mu RV) \left[ \int_{\Omega_D \cap \Omega_{*R}} p_R(x) dx - \int_{\Omega_{*D} \cap \Omega_R} p_R(x) dx \right] \\
 &\quad + \mu DY \left[ \int_{\Omega_R \cap \Omega_{*D}} p_D(x) dx - \int_{\Omega_{*R} \cap \Omega_D} p_D(x) dx \right] ,
 \end{aligned}$$

where in the first bracket

$$\Omega_D = \Omega_D \cap \Omega_{*R} + \Omega_D \cap \Omega_{*D} ,$$

$$\Omega_{*D} = \Omega_{*D} \cap \Omega_R + \Omega_{*D} \cap \Omega_D , \text{ and}$$

the latter two regions cancel each other out. A similar argument applies to the second bracket. Collecting integrals over the same region yields

$$J - J^* = (1 - \mu RV) \int_{\Omega_D \cap \Omega_{*R}} [p_R(x) - \lambda^* p_D(x)] dx \\ + (1 - \mu RV) \int_{\Omega_R \cap \Omega_{*D}} [\lambda^* p_D(x) - p_R(x)] dx \quad ,$$

$$\text{where } \lambda^* = \frac{\mu DY}{1 - \mu RV} \quad , \quad \text{or}$$

$$\mu DY = \lambda^* (1 - \mu RV) \quad .$$

But in the first integral

$$\Omega_{*R} \cap \Omega_D \subseteq \Omega_{*R} \quad ,$$

$$\Lambda(x) = \frac{p_R(x)}{p_D(x)} \geq \lambda^* \quad , \quad \text{or}$$

$$p_R(x) - \lambda^* p_D(x) \geq 0$$

by definition of region  $\Omega_{*R}$ . And in the second integral

$$\Omega_{*D} \cap \Omega_R \subseteq \Omega_{*D} \quad ,$$

$$\Lambda(x) = \frac{p_R(x)}{p_D(x)} \leq \lambda^* \quad , \quad \text{or}$$

$$\lambda^* p_D(x) - p_R(x) \geq 0$$

by definition of  $\Omega_{*D}$ .

Thus,  $J - J^* \geq 0$ , or equivalently,  $J^*$  is a minimum provided  $1 - \mu RV > 0$ . The Lagrange multiplier must be sufficiently small so that the interceptor cost does not outweigh the leakage cost in our augmented cost function.

Finally, note that the optimal  $\Omega_{*R}$  is chosen so that  $\Omega_{*R} = \{x: \Lambda(x) \geq \lambda^*\}$ , which then is equivalent to  $\Omega_{*R} = \{x: L(x) \geq \lambda^*\}$ , where  $L(x)$  is the LLR function.

Notice that  $\Omega_{*R}$  may consist of many disjoint regions and may also cross discontinuities of  $p_R(x)$  and  $p_D(x)$ . The decision threshold  $\partial \Omega_{*R}$  consists of all those points  $x$  that have the same value of  $\Lambda(x)$ , namely,  $\lambda^*$ . This is true regardless of which component region of the domain of  $p_R(x)$  or  $p_D(x)$  that the observation falls into. This result gives the theoretical basis for the so-called synchronized thresholds for sensors in series.

## APPENDIX D

### THE SYNCHRONIZED FIRING THRESHOLD

In this appendix the method used to obtain the leakage/interceptor ( $P_L$  vs  $I$ ) performance curves of Section 4.1 for two sensors in series is outlined. The method detailed here can be readily extended, in principle, to a series chain of three or more sensors using the density function derived in Appendix B. We add the qualifier "in principle" because although the technique is straightforward, the numerical integrations taking place over regions of higher and higher dimensionality become prohibitive. However, a dimension reduction technique is under investigation that will reduce analyses of sensor chains to vector spaces of one or two dimensions.

The  $P_L$  vs  $I$  performance curves are obtained by employing a single moving firing threshold or a pair of synchronized thresholds based on the value of the log-likelihood ratio (LLR), as derived in Appendix C. In Appendix C it was shown that, regardless of the form of the RV and decoy density functions (provided that they indeed are density functions), the boundary  $\partial\Omega_R$  of the decision region of whether to call an object an RV or a decoy is given by  $L(x) = \text{constant}$ , where the constant depends on the inventory level.  $L(x)$  is the LLR function defined by

$$L(x) = \log \left[ p_R(x) / p_D(x) \right] , \quad (\text{D.1})$$

where  $x$  is the discriminant vector in the joint feature space. The boundary  $\partial\Omega_R$  is precisely the firing threshold.

This firing rule is true independently of whatever rule is used to determine the traffic threshold of sensor  $S_1$ . In other words, given any particular traffic rule, Equation (D.1) yields the optimal firing thresholds. This condition is so because we allowed the RV and decoy densities to be arbitrary, possibly discontinuous, probability density functions in the derivation of the optimal  $\partial\Omega_R$ . A traffic threshold will induce discontinuities in  $p_R(x)$  and  $p_D(x)$  in the joint feature space, as is shown below.

The optimal firing rule is now applied to the single threshold traffic model discussed in Section 3. The figures and discussion here are tailored to classical Gaussian sensors. In joint feature space  $(x_1, x_2)$ , equiprobable contours for the RV and decoy densities are shown in Figure D-1. Given some traffic capacity for sensor  $S_2$ , we assume the appropriate threshold  $\tau$  is chosen. The threshold corresponds to some LLR value  $L(x_1)$  defined on the  $x_1$  axis; call it  $L(x_1) = a$ . Because objects whose  $x_1$  discriminant lies to the left of  $\tau$  are not measured by sensor  $S_2$ , they have no  $x_2$  measurement associated with them. Thus, the RV and decoy probability density functions in the  $(x_1, x_2)$  plane are Gaussian functions of  $x_1$  only if  $x_1 \leq \tau$ . Accordingly, their equiprobable contour lines must be straight lines parallel to the  $x_2$  axis. To the right of the threshold they are joint Gaussian densities of both  $x_1$  and  $x_2$ . (To the left of the threshold, the circular contours have been retained as dashed curves to give a sense of scale to the spacing of the vertical equiprobable lines.)

The RV and decoy densities in the joint feature space are discontinuous along the line  $x_1 = \tau$ . The LLR value for any measured object can be based on only the available information; therefore, for any feature vector  $x = (x_1, x_2)$

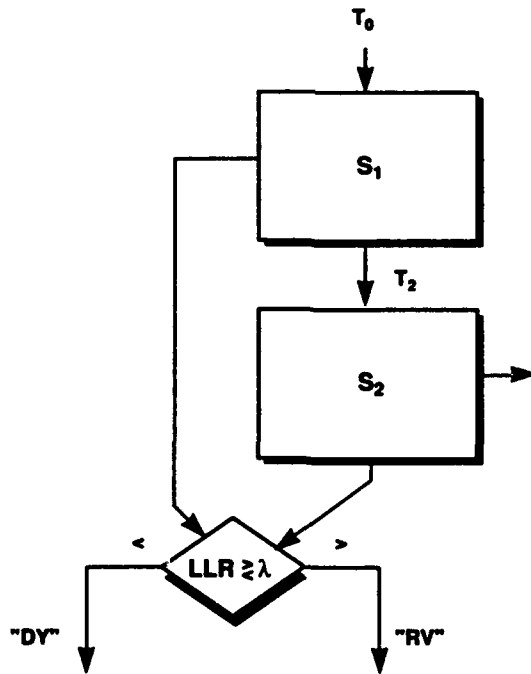
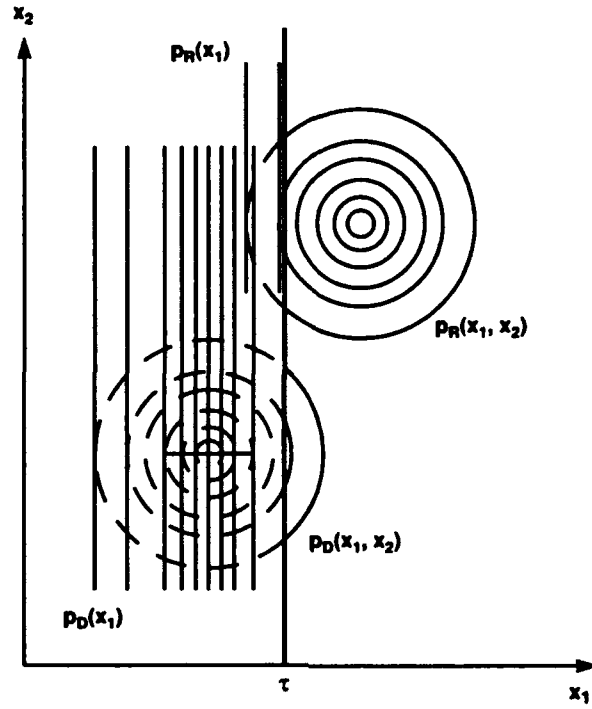


Figure D-1. Discontinuous density functions induced by a traffic threshold.

$$\begin{aligned}
L(x) &= L(x_1) = \log \left[ p_R(x_1) / p_D(x_1) \right] x_1 \leq \tau, \text{ and} \\
L(x) &= L(x_1, x_2) = \log \left[ p_R(x_1, x_2) / p_D(x_1, x_2) \right] x_1 > \tau.
\end{aligned}
\tag{D.2}$$

Thus,  $L(x)$  is used in the dual context of Equation (D.2) and will always be based on the maximum available feature information.

The sequence of firing thresholds shown in Figure D-2 illustrates how thresholds move across the feature space as the inventory is increased on the  $P_L$  vs  $I$  curve. The curve from Figure 11 that represents the bulk filter and precision sensor in series has been reproduced. In the sequence of diagrams, the two-dimensional contours are drawn for visual purposes only; too many vertical lines would tend to clutter the figures.

Figure D-2(a) shows the location of the firing threshold  $\eta$  for a very low inventory. Threshold  $\eta$  is the locus of points satisfying  $L(x_1, x_2) = \alpha_1$  for some constant  $\alpha$ . The constant  $\alpha_1$  is chosen so that the total number of objects, RVs and decoys, whose discriminant vectors lie in the infinite wedge bounded by  $\tau$  [ $L(x_1) = a$ ] and  $\eta$ , will be equal to the inventory  $I_1$ . Once  $\alpha_1$  is determined, if the RV density is integrated over this same region, the corresponding leakage is obtained; actually,  $1 - P_L$  is obtained.

As the inventory is increased to  $I_2$ , the firing threshold  $\eta$  moves down to  $L(x_1, x_2) = \alpha_2$ , as shown in Figure D-2(b). By continuing to increase  $I$ ,  $I_3$  is finally reached, as shown in Figure D-2(c), where  $L(x_1, x_2) = \alpha_3 = a$  ( $a$  is the value of the traffic threshold). This is a critical value for the firing threshold. From this point on, as  $\alpha$  is decreased (by increasing  $I$ ), a second firing threshold  $\eta'$  will begin to move across the left half of the feature space starting at the traffic threshold [see Figure D-2(d)]. Notice that the value of  $L(x_1) = \alpha_4$  on  $\eta'$  is the same as  $L(x_1, x_2) = \alpha_4$  on  $\eta$ . All of the points lying in the infinite strip bounded by  $\eta'$  and  $\tau$  and in the infinite wedge bounded by  $\eta$  and  $\tau$  have an LLR value greater than  $\alpha_4$ , where the LLR value depends upon all the known information:  $x_1$  only in the strip and  $(x_1, x_2)$  in the wedge. This collection of points forms the region  $\Omega_R$  for the inventory  $I_4$ . Finally, as the inventory is increased, the two thresholds  $\eta'$  and  $\eta$  move in a synchronized manner to the left/downward, satisfying  $L(x_1) = \alpha_i = L(x_1, x_2)$ , as indicated in Figure D-2(e). By the time the inventory reaches the size of the threat, the synchronized thresholds have moved across the entire feature space.

As an example, to obtain the leakage for Figure D-2(d) we let

$$f(x_1) = p_R(x_1) \text{ and } g(x_2) = p_R(x_2)$$

be the RV density functions for sensors  $S_1$  and  $S_2$ , respectively. We want to compute the following probabilities:

$$\Pr(\alpha_4 < x_1 < a) \text{ and } \Pr(x_1 + x_2 > \alpha_4, x_1 > a).$$

The sum of these two probabilities is  $1 - P_L$ . The first is the fraction of RVs whose discriminant lies in the infinite strip; the second is the fraction of RVs whose discriminant lies in the infinite wedge. Using the notation of Appendix B, they are given by

$$\int_{\alpha_4}^a f(x_1) dx_1 \text{ and } \int_a^\infty \left[ \int_{\alpha_4}^\infty g(x_2 - x_1) f(x_1) dx_2 \right] dx_1.$$

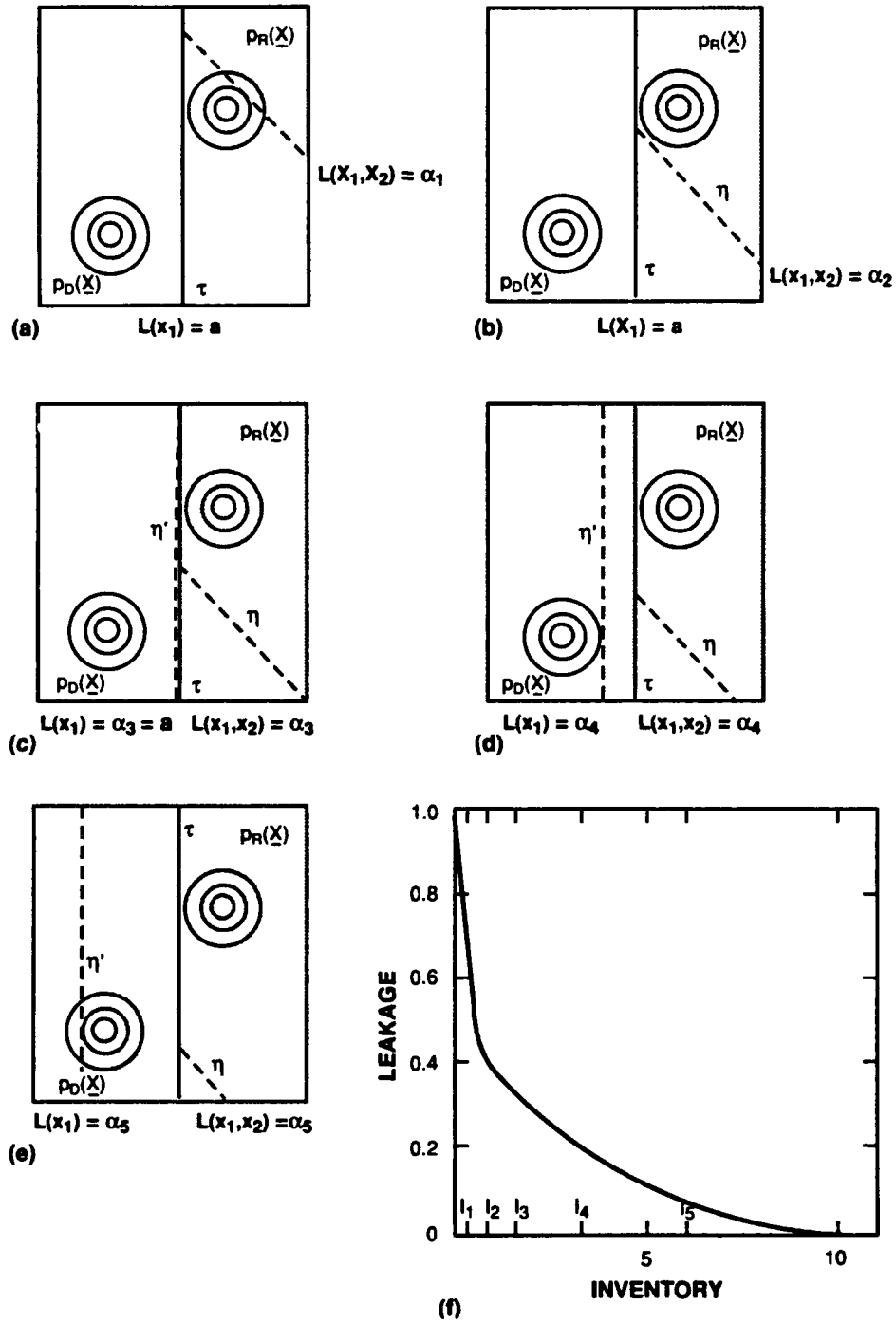


Figure D-2. Synchronized firing thresholds.

## REFERENCES

1. R. B. Holmes and S. M. Rocklin (private communication, 1990).
2. R. B. Holmes and S. M. Rocklin, "Performance modeling of multisensor networks," *International Society for Optical Engineering Proceedings SPIE*, Orlando, Florida (1990), vol. 1306.

# REPORT DOCUMENTATION PAGE

*Form Approved*  
**OMB No. 0704-0188**

Public reporting burden for this collection of information is estimated to average 1 hour per response, including the time for reviewing instructions, searching existing data sources, gathering and maintaining the data needed, and completing and reviewing the collection of information. Send comments regarding this burden estimate or any other aspect of this collection of information, including suggestions for reducing this burden to Washington Headquarters Services, Directorate for Information Operations and Reports, 1215 Jefferson Davis Highway, Suite 1204, Arlington, VA 22202-4302, and to the Office of Management and Budget, Paperwork Reduction Project (0704-0188), Washington, DC 20503.

1. AGENCY USE ONLY (Leave blank)	2. REPORT DATE 12 August 1992	3. REPORT TYPE AND DATES COVERED Technical Report	
4. TITLE AND SUBTITLE <b>Sensors in Series: A Study of Sensors with Limited Traffic Capacity</b>		5. FUNDING NUMBERS  C — F19628-90-C-0002 PR — 359	
6. AUTHOR(S)  Sol M. Rocklin and Jeffrey W. Tolleson			
7. PERFORMING ORGANIZATION NAME(S) AND ADDRESS(ES)  Lincoln Laboratory, MIT P.O. Box 73 Lexington, MA 02173-9108		8. PERFORMING ORGANIZATION REPORT NUMBER  TR-943	
9. SPONSORING/MONITORING AGENCY NAME(S) AND ADDRESS(ES)  SDIO The Pentagon Washington, DC 20301		10. SPONSORING/MONITORING AGENCY REPORT NUMBER  ESC-TR-91-177	
11. SUPPLEMENTARY NOTES  None			
12a. DISTRIBUTION/AVAILABILITY STATEMENT  Approved for public release; distribution is unlimited.		12b. DISTRIBUTION CODE	
13. ABSTRACT (Maximum 200 words)  <p>This report examines the discrimination capability of a network of two sensors connected in series. A model of a traffic-limited sensor is developed and then used to quantify the deleterious effect of high traffic levels on the performance of the sensor. Various combinations of two sensors are compared, and for moderate inventory levels, a low-quality bulk filter followed by a high-quality, traffic-limited precision sensor yields the best performance.</p>			
14. SUBJECT TERMS sensors                      traffic-limited sensor                      leakage discrimination              bulk filter    RV series network                precision sensor                                decoy			15. NUMBER OF PAGES 64
			16. PRICE CODE
17. SECURITY CLASSIFICATION OF REPORT  Unclassified	18. SECURITY CLASSIFICATION OF THIS PAGE  Unclassified	19. SECURITY CLASSIFICATION OF ABSTRACT  Unclassified	20. LIMITATION OF ABSTRACT

**END  
FILMED**

**DATE:**

*11-92*

**DTIC**